Available online at www.sciencedirect.com
ScienceDirect
Journal of the European Ceramic Society 30 (2010) 1555–1577
www.elsevier.com/locate/jeurceramsoc

Review

Micrometer and nanometer-scale parallel patterning of ceramic and organic–inorganic hybrid materials

Johan E. ten Elshof*, Sajid U. Khan, Ole F. Göbel

University of Twente, MESA+ Institute for Nanotechnology, P.O. Box 217, 7500 AE Enschede, The Netherlands

Received 19 August 2009; received in revised form 6 January 2010; accepted 10 January 2010
Available online 1 February 2010

Abstract

This review gives an overview of the progress made in recent years in the development of low-cost parallel patterning techniques for ceramic materials, silica, and organic–inorganic silsesquioxane-based hybrids from wet-chemical solutions and suspensions on the micrometer and nanometer-scale. The emphasis of the discussion is placed on the application of soft-lithographic methods, but photolithography-aided patterning methods for oxide film growth are also discussed. In general, moulding-based patterning approaches and surface modification-based patterning approaches can be distinguished. Lateral resolutions well below 100 nm have been accomplished with some of these methods, but the fabrication of high-aspect ratio patterns remains a challenge.

Keywords: Patterning; Moulding; Ceramic; Thin film; Soft lithography

Contents

1. Introduction

The miniaturization of objects and device components down to the micron- and nanometer-scale, and the development of methods to fabricate and register these, presents one of the main

* Corresponding author. Tel.: +31 534892695; fax: +31 534893595.
E-mail address: j.e.tenelshof@utwente.nl (J.E. ten Elshof).

0955-2219/$ – see front matter © 2010 Elsevier Ltd. All rights reserved.
doi:10.1016/j.jeurceramsoc.2010.01.016

technological trends of the last decade, and has been reported in a large number of reviews, *e.g.*, Refs. 1–6.

Among these methods, a number of alternative techniques to traditional photolithography for patterning a variety of materials have been developed. Photolithography is commonly used in the electronics industry and has been under development for many decades. At present, feature sizes $\ll$100 nm can be patterned in silicon on large scale. However, the drawbacks of the techniques are that high-end equipment and clean room conditions are required, and the methodology is applicable only to a narrow set of materials.

In an attempt to overcome these restrictions, a family of related patterning techniques was developed by the Whitesides Group at Harvard University in the 1990s.[7–9] These so-called soft lithography techniques are mainly parallel patterning methods, so large areas can be patterned in a relatively short period of time. They may provide cheap alternatives for the much more costly photolithographic processes, and are able to process a wider range of materials, including polymers, biomaterials, ceramics, hybrids, and composites. At least with some of these techniques, parallel patterning on sub-100 nm scale is possible. Since their development, soft-lithographic techniques have achieved widespread use in academic and industrial laboratories for applications in diverse fields, *e.g.*, photonics, biotechnology, microfluidics, and electronics. While most of these research efforts were focused on the patterning of polymers, biomaterials and self-assembled monolayers, it has also found application in the micrometer and submicrometer patterning of ceramics and organic–inorganic hybrid materials,[10] and that is the main topic of this review.

All soft lithography techniques require an elastomeric mould or stamp that is patterned with a relief structure on its surface. One of the steps in the patterning process involves bringing the elastomer into conformal contact with a substrate, and be used as stamp or mould.[9] The patterned elastomer is made by casting a liquid prepolymer onto a 3D patterned master structure,[11] followed by polymerization of the prepolymer. In most cases the master structure is made from silicon or photo resist and obtained by conventional photolithography. The most popular and widely used elastomeric material is polydimethylsiloxane (PDMS), a rubber-like material with a low surface energy that can be easily peeled off the master after cross-linking. To aid in the debonding process, the silicon master is usually silanized in order to make it hydrophobic prior to use. The final result is an elastomeric negative replica of the master structure with three-dimensional patterns. Essentially, the patterned elastomer can be utilized for patterning in two different ways: (1) the protruding patches of the patterned elastomer can be employed to carry a precursor ink to the substrate (printing approach), or (2) precursor material is contained in the recessed regions between the protruding patches (moulding approach). These two strategies will be discussed in more detail in Section 2.1. In either case, the precursor is transferred to the substrate, and the stamp or mould aids in defining the locations where precursor material is deposited. For proper transfer of material, it is necessary that the stamp or mould makes good conformal contact with the substrate.

The inability of soft lithography for registry of formed patterns, *i.e.*, the impossibility to position a structure on a predefined location, could be one of the main hurdles to the application of soft-lithographic patterning in industry. It makes fabrication of more complex multiple layer patterns rather complicated. Some efforts have been made to combine the versatility of soft lithography with the registration tools developed for photolithography.[12] Other researchers have proposed strategies to use photolithography itself instead to define the pattern. Such strategies will be discussed here as well, as they may present a viable approach to industrial parallel patterning of ceramics and hybrids on length scales that are only limited by the resolution of the photolithographic process.

A general review on submicrometer-scale parallel patterning of ceramic materials was published in 2004 by the Aksay Group at Princeton.[10] More focused reviews on site-selective liquid-phase deposition of ceramics via photolithography-aided patterning techniques were published by Masuda, Koumoto and co-workers.[13,14]

The current review addresses low-cost micron and submicron-scale parallel patterning methods, with emphasis on the formation of patterned thin films of solid state materials, more specifically metal oxides and organic–inorganic silsesquioxane-based hybrid materials. It is motivated by the ongoing activity on the subject over the last years. The main focus of the current review will be on materials that can be deposited and patterned by liquid precursors, such as sol–gel solutions and colloidal suspensions. Polymers, metals[11] and colloidal assemblies[15–17] are outside the scope of this paper. With a very few exceptions, neither does it address serial patterning methods, such as ink jet printing,[18] dip-pen nanolithography,[19–21] direct ink writing,[22] nor ion-beam and e-beam methods.[2]

An overview of the principles of the most commonly used parallel patterning methods is presented in Section 2.1. Section 2.2 addresses the conflicting properties required for soft-lithographic stamps and moulds. The inks, molecular precursor solutions and particle suspensions used in patterning, and their underlying chemistries are described in Section 2.3. Viscosity, surface tension, solids content, and type of solvents are the most important properties of these precursors. Sections 3 and 4 give an overview of the progress made in recent years on submicrometer-scale patterning of functional ceramics and hybrid materials by moulding-based and surface modification-based (printing) approaches, respectively. Some general conclusions are drawn in Section 5.

2. Principles of soft-lithographic patterning

2.1. Soft lithographic and lithographic techniques

Most of the patterning techniques that will be discussed in this review belong to the family of soft-lithographic processes.[9,11] The methods that are applicable to ceramics and hybrid materials can be divided into two main categories, namely moulding-based approaches and surface modification-based approaches.[10]

Moulding-based patterning approaches and their application to forming ceramic and hybrid micro- and nanopatterns are discussed in Section 3. They include conventional micromoulding, microtransfer moulding, and micromoulding in capillaries. They all employ physical confinement of a liquid precursor solution or suspension to define the shape of the final pattern. They produce a negative replica of the pattern in the mould, and a positive replica of the original lithographic master. At least in principle high-aspect ratio structures can be made by these approaches.

PDMS is permeable to many solvents but not to polymers or nanoparticles, so physical drying of a moulded solution or suspension is possible by diffusion of the solvent into the PDMS mould. The precursor dries slowly and solidifies while it is still confined by the mould.[23] The resolution of the patterned material is determined by the surface energies of the components, and the ability of the mould to detach from the patterned material after drying. High resolution requires the selection of a mould material that has significantly lower adhesion energy with the pattern material than the substrate has with the material. After removal of the mould, the patterned material can be heat-treated, *e.g.*, pyrolized, in order to obtain the final phase.

In microtransfer moulding (μTM),[9] shown in Fig. 1a, the precursor solution is deposited in the recessed regions of a patterned mould. Excess material on the protruding parts is removed and the mould is brought into conformal contact with a substrate. After a certain period of time, during which the precursor dries by solvent removal (physical drying) and/or condensation of precursors into –inorganic– polymeric networks (chemical drying), the mould is removed. If the adhesion to the (PDMS) mould is smaller than that to the substrate, the patterned material remains attached to the substrate, and can be given a final heat treatment.

The micromoulding (embossing) process shown in Fig. 1b involves imprinting a patterned mould into a continuous wet film by application of some pressure. Both soft (PDMS) and rigid (glass, poly(methyl methacrylate)) materials have been employed for the moulds. The technique can pattern well in the sub-50 nm scale,[24,25] a resolution that has not been met by any of the other techniques discussed in this review. The formation of a residual layer between the desired features of the patterns is inherent to the technique. This is why it is especially interesting for applications in which the presence of residual layers presents no problem. In other cases, a post-etching step after pattern formation is required.

An often used alternative term for micromoulding is nanoimprint lithography (NIL).[26] Although NIL traditionally focuses on nanopatterning of polymers and is often done at elevated temperatures to reduce viscosity, and optionally involves a final UV curing step, the process is essentially similar to micromoulding. Micromoulding and microtransfer moulding are both fast parallel patterning processes with which large areas can be patterned.

The idea behind micromoulding in capillaries (MIMIC)[27] is that the formation of residue layers is avoided. The process is schematically shown in Fig. 1c. A clean patterned mould is brought into conformal contact with the substrate before the liquid precursor is supplied. A network of empty microcapillary channels forms in the mould. A precursor solution is then supplied to the entrances of the capillaries at the side of the mould. The precursor solution is drawn into the microchannels by capillary force. In principle, no residue layer can form in areas where adhesive conformal contact between mould and substrate is already established. MIMIC is a semi-parallel patterning process. It takes time for the precursor fluid to fill the entire pattern under the mould. For example, the Washburn equation predicts that the penetration rate of water in a straight 1 μm diameter channel at 298 K is such that its penetration length is 1.5 mm after 1 s, but only 10 mm after 50 s. In narrower channels the penetration rate is even lower and becomes impractical for most purposes. It is clear that such kinetic factors will play a role in determining the quality of the final pattern.

In the surface modification-based patterning approaches first a chemically contrasted substrate is generated. This can be accomplished in various ways, as will be discussed in Section 4 in more detail. After that a layer is grown or material deposited selectively on those patches of the substrate which have proper surface chemistry. Examples of chemical contrasts are hydrophobic–hydrophilic contrast (electrical) charge contrast, and chemically specific contrasts such as catalytic activity for transformation of one or more of the components in the precursor solution into solids.

Since the surface modification methods do not rely on physical confinement, the ultimate lateral resolution of the method is lower than what can be accomplished by moulding-based methods. The height of the formed oxide patterns is usually in the range of 20–80 nm, so the aspect ratios are quite low.

A general soft-lithographic surface modification approach is microcontact printing (μCP),[7] shown in Fig. 1d, with which the chemistry of a surface can be locally modified. Chemically contrasted substrates are made by printing self-assembled monolayers or very thin multilayers of an ink that was carried to the substrate by the stamp and is transferred by conformal contact. Well-known examples are octadecyl trichlorosilane (OTS; $Cl_3Si–C_{18}H_{37}$) on silicon oxide and octadecanethiol ($C_{18}H_{37}–SH$) on gold. They yield a thin multilayer and self-assembled monolayer after drying, respectively, and both are very hydrophobic.[2] When the substrate is exposed to a particle suspension or chemical solution, heterogeneous nucleation and growth of oxide precursors occurs more readily on polar (hydrophilic) surface patches. The adhesion of oxide nanoparticles or inorganic polymers to a surface is also favoured by the presence of polar groups at the surface. Hence, hydrophobic patches on a substrate inhibit the local formation of a ceramic phase, which can be exploited to generate local patterns of ceramics on the other, *i.e.*, the more hydrophilic patches.

The confocal contact printing method in Fig. 1e is technically simple. The precursor is directly printed onto a substrate in a single patterning step. However, the disadvantage is that the resolution and quality of replication of the pattern are controlled entirely by the rheological properties of the precursor ink and the drying rate, which requires careful engineering of the precursor solution. In microcontact printing-based approaches the functions of pattern definition and film formation are carried out by different components. This makes optimization of the patterning process easier, since they involve two independent

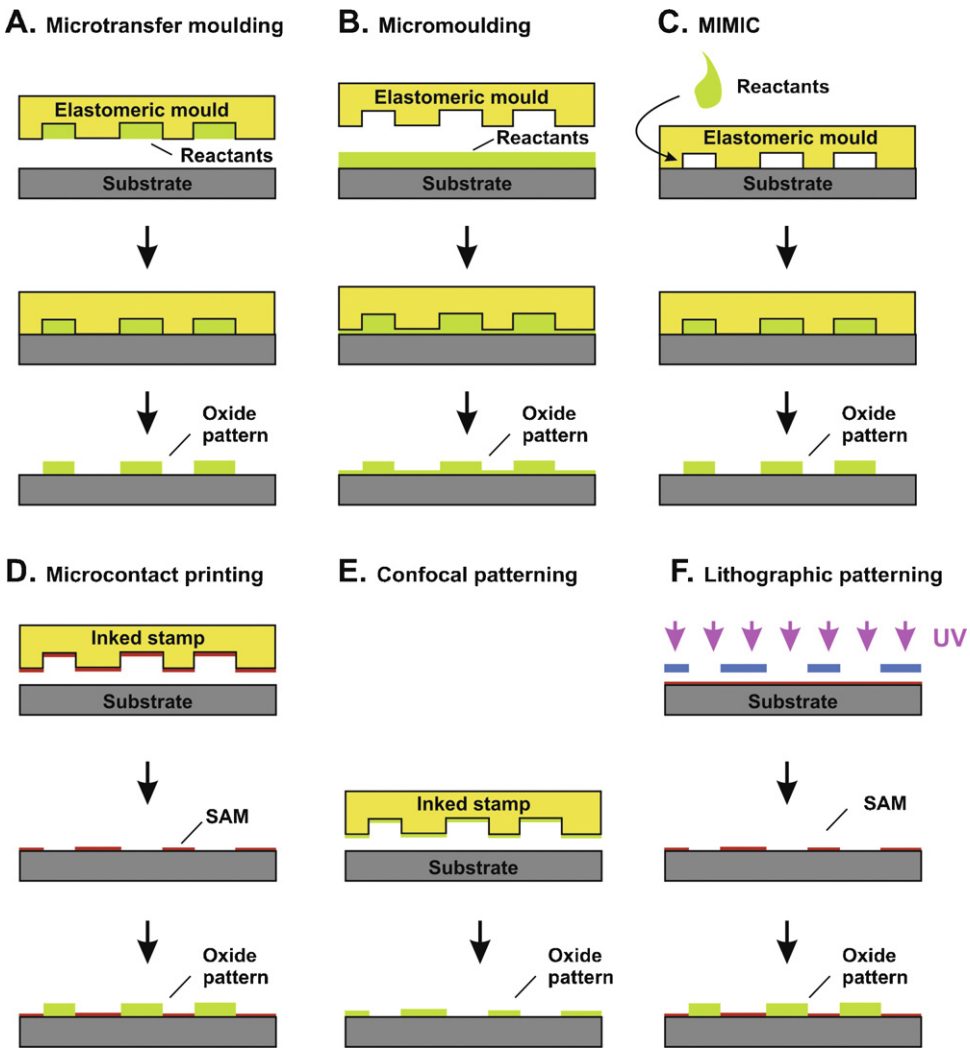

Fig. 1. Soft lithographic (a–e) and hard lithographic (f) patterning processes. (a) Microtransfer moulding; (b) micromoulding/nano imprint lithography; (c) micromoulding in capillaries; (d) microcontact printing of self-assembled monolayer or multiple layer (SAM); (e) confocal patterning; (f) lithographic patterning of SAM.

steps. In practice, the resolution of confocal printing is much higher than 50 μm.[28] However, much smaller pattern features could be possible once a better control of the solution chemistry and the printing conditions is established.

One of the limitations of soft-lithographic patterning techniques in general concerns the registry of the formed patterns.[10] Therefore, it remains problematic to fabricate hierarchical structures with a more complex function by combining several patterning steps in sequence. This is one of the reasons why several investigators have explored possibilities to micropattern ceramic materials by a conventional hard lithography-supported approach. Photolithography-aided patterning, illustrated in Fig. 1f, uses the tools of photolithography, a well-known technology that has been developed over the last decades for silicon technology and microelectronics. It involves exposing a substrate to UV light via a shadow mask, so that only certain parts of the substrate are actually exposed. The UV energy can be employed either to generate chemically contrasted substrates (prior to film deposition or growth) by selectively decomposing a preformed SAM, or locally transform UV sensitive ceramic precursors into a condensed phase. The resolution of the whole process is in principle limited only by that of the photolithographic process. An advantage of this approach is that the presently available technology developed for conventional photolithography can be used to transfer patterns. All required equipment and UV photomasks are readily available.

2.2. Properties of elastomer materials

All soft lithography techniques depend on surface topographical relief patterns of elastomeric stamps and moulds. Of these, PDMS made from Sylgard 184 (Dow Corning Inc.) is the most popular type of polydimethylsiloxane for making soft-lithographic stamps. It combines flexibility and conformal contact to an extent that is sufficient for many processes. Sylgard 184 consists of a silicone resin cross-linked by a mixture of vinyl-terminated PDMS and trimethylsiloxy-terminated poly(methylhydro-siloxane) polymers. The resulting material has a highly cross-linked three-dimensional structure. It offers a high elongation at break (>100%).

When used for confocal patterning, intimate contact with the substrate is achieved locally at the protruding areas, while a gap remains between the substrate and the recessed areas. Essentially, this requires the stamp (or mould) to have two conflicting properties with respect to its Young's modulus. On the one hand, the stamp should be soft enough to enable good conformal contact with the substrate. It should adapt elastically to small substrate surface variations (roughness) and not leave any voids between stamp and substrate. This requires a low Young's modulus and high work of adhesion. On the other hand, a precise definition of micropatterns requires a rigid material. This implies a high Young's modulus.[29] The conflict between these two properties sets a limit on the resolution that can be achieved with soft elastomeric stamps with good conformal contact.

Various authors have pointed out that deformation of soft stamps may lead to various kinds of collapse of the pattern, *e.g.*, Ref. 30. For example, in rubber stamps with low aspect ratio patterns, where the protruding features are widely interspaced, so-called roof collapse may occur, in which the recessed areas deform to such an extent that they touch the substrate. Quantitative criteria against roof collapse have been proposed.[31] On the other hand, soft stamps with high-aspect ratio structures suffer from buckling, pairing and collapse to the ground. It has been proposed that decreasing the work of adhesion between stamp and substrate helps to prevent ground collapse,[32] and increasing the pattern density was found to be beneficial for pattern transfer fidelity.[33]

The use of composite stamps with a stiff backbone and a soft patterned layer may improve pattern quality,[34] but increasing the stiffness of the stamp will remain crucial for the definition and stability of patterns at ultimate resolution in many processes.[29] Also, when preceramic suspensions are used, harder masks that are less prone to deformation are preferred as they will withstand increased pressures with less deformation.

Another problem with PDMS is its interaction with certain organic solvents. Lee, Park, and Whitesides investigated the compatibility of PDMS with a wide range of solvents, and considered three aspects of compatibility, namely (i) the swelling of PDMS in a solvent, (ii) the partitioning of solvent between PDMS and solvent phase, and (iii) the dissolution of small oligomeric fragments of PDMS in the solvent.[23] Of these three, swelling was found to exert the largest influence. Among the solvents that swelled PDMS the least were water, glycerol and ethylene glycol. Highly swelling solvents were very apolar solvents such as pentane and xylene.

The resolution achievable with standard PDMS, made from Sylgard 184, has often been limited to >100 nm because of the low compression modulus of 2 MPa.[35] The use of a harder version of PDMS, called hard-PDMS or h-PDMS, with a compression modulus of 9 MPa has increased the resolution to 50 nm, but not for densely spaced features, or high-aspect ratio patterns.

h-PDMS is prepared from trimethylsiloxy-terminated vinylmethylsiloxane-dimethylsiloxane (VDT-731; Gelest) and methylhydrosiloxane-dimethylsiloxane (HMS-301; Gelest) copolymers. The h-PDMS system has cross-linkers that have relatively short lengths as compared to those in Sylgard 184 PDMS. Composite bi-layer patterning elements that use a thin patterned layer of h-PDMS with a thick back layer of Sylgard 184 PDMS effectively combine some of the attractive features of these two materials for certain applications.[36]

Rigid moulds made of quartz may stick to the imprinted materials unless they have been treated with an anti-sticking release layer. Polymers such as poly(methyl methacrylate) (PMMA) can also be used as a mould material, however an anti-sticking treatment using low surface energy materials such as fluorosilane self-assembled monolayer is still needed for easy release. Several alternative polymeric materials have been proposed for use in stamps, *e.g.*, Refs. 35–37. Some examples are listed in Table 1. In recent years a number of fluorinated polymers have been developed for use in stamps.[38–42] They exhibit good mechanical properties, while having a lower surface energy ($\gamma < 20\ mJ/m^2$) than PDMS ($\gamma = 21.6\ mJ/m^2$), and being less prone to swelling by solvents.

Other essential properties of the stamp or mould are its surface energy and the nature of any present surface functional groups, because these determine the wetting and dewetting behaviour of precursor solutions in the mould, as will be elaborated in more detail below for the respective techniques. Sylgard 184 PDMS is hydrophobic, *i.e.*, water has a contact angle >90° and does not spread on the surface of PDMS. While this may be advantageous for the debonding step in micromoulding and microtransfer moulding, as will be discussed in Section 2.4, it is disadvantageous when a MIMIC process for aqueous solutions is targeted, because water will probably not want to enter a predominantly hydrophobic micron-sized capillary. A variety of methods has been proposed to alter the chemical properties of PDMS. The simplest and most commonly used method to make the surface of PDMS hydrophilic is by an oxygen plasma treatment for periods of a few tens of seconds.[43] The resulting surface modification

Table 1
Comparison of Young's modulus, elongation at break, toughness and shrinkange upon polymerization in a nanoimprint lithography mould. Data taken from Refs. 36, 38.

Mould material	Tensile modulus (MPa)	Elongation at break (%)	Toughness (MPa)	Shrinkage (%)
PDMS (Sylgard 184)	1.6–1.8	146–160	4.77	1.1
Hard-PDMS	8.2	6.5–7.0	0.02	1.6
Soft-PDMS	0.6	70	0.13	3.1
hv-PDMS[36]	3.4	54	0.41	0.6
Fluorinated hybrimer[38]	33.5–40	5.3	1.12	2–2.5
Flexible fluorinated hybrimer[38]	32.5	30	4.5	2–2.5

is consistent and reproducible, yielding contact angles <5°, and requires no special chemicals. The oxygen plasma oxidizes the surface of PDMS, so that a thin hydrophilic SiO_x layer with surface silanol groups Si–OH form. Unfortunately, it is well known that the hydrophilic modification is not permanent. In the course of time, typically hours, low molecular weight siloxane residuals migrate to the surface and cover the SiO_x layer with a low surface energy film, so that the surface becomes hydrophobic again. The same residuals are responsible for the reported contamination of substrate surfaces during conformal contact. Detailed studies have shown that silicone-related material is transferred from flat stamps, and even more material is transferred from patterned stamps.[44] Silicone transfer can be minimized by curing the PDMS stamps at elevated temperatures, but also depends on the pretreatment of the stamp and the type of ink used.[45,46] Furthermore, it has been suggested that the transferred material also contains traces of platinum, which are present in Sylgard 184 as cross-linking catalyst.[46] No fast and easy method is known that can completely and permanently remove these residuals from the stamp. An exhaustive week-long cleaning procedure has been proposed that yields PDMS stamps containing no or very little oligomer material.[47] However, the hydrophobic recovery after oxygen plasma treatment of cleaned PDMS stamps is only slightly affected when stored in air. This suggests that the stamps probably regain their ability to contaminate and transfer PDMS residues.[46]

Alternative ways to modify the stamp's surface energy more permanently are through chemical modifications, for which several routes have been proposed. Sol–gel coatings based on titanium alkoxide, zirconium alkoxide and vanadium alkoxide have been reported.[48] Also thiol, amine, sulfonic acid and cyano-functional coatings have been applied on PDMS.[49–51] In these cases the PDMS surface was first plasma-treated to form silanol groups to which the sol–gel precursors could attach. Modification with plasma-polymerized acrylic acid yielded hydrophilic PDMS surfaces for several days,[52] and a poly(urethaneacrylate) coating was shown to lead to a significantly reduced rate of swelling by solvent absorption.[53]

2.3. Precursor formulations

Any physically drying sol–gel system, dispersion, polymeric, colloidal, or ionic solution can in principle be used as a precursor for patterning. Essentially, homogeneous solutions and particle suspensions can be distinguished. The components in the precursor "ink" should be at least approximately one order of magnitude smaller than the feature sizes of the pattern. The other requirements for the precursor depend on the actual patterning process.

Different chemistries have been utilized to make precursor formulations for pattering. They are essentially similar to the chemistries that are employed for wet-chemical processing of ceramic thin films.[54–56] Especially sol–gel chemistry, metal–organic decomposition (MOD), and chemical bath decomposition (CBD) are popular. Apart from achieving a high solids content in solution, which is not possible in combination with low viscosity, these chemistries can easily meet most of the other requirements mentioned above. Only in cases where patterns with a high-aspect ratio are required, or the chemical transformation from liquid precursor to final ceramic phase has to be avoided, suspension-based precursors are preferentially utilized.

Sol–gel processing. This is the most commonly used chemistry for precursor solutions. Sol–gel alkoxide chemistries can be divided into two classes, depending on whether or not the element silicon is involved.[57] In silicon alkoxide chemistry, hydrolysis and condensation of molecular precursors $Si(OR)_4$ or $R'–Si(OR)_3$ into condensed prepolymers proceeds via the following two fundamental reactions:

$$\text{Hydrolysis}: \quad \text{=Si–OR} + H_2O \xrightarrow{H^+} \text{=Si–OH} + \text{ROH}$$

$$\text{Condensation}: \quad \text{=Si–OH} + \text{HO–Si=} \xrightarrow{H^+} \text{=Si–O–Si=} + H_2O$$

Here R represents an alkyl group, and R′ an arbitrary side group that can carry virtually any functionality. The reactions are catalyzed by protons and hydroxyl groups. This chemistry has been employed for making low-*k* dielectrics, such as porous silicas and organosilicas. The reactions are usually carried out in alcoholic solution with some water added, see *e.g.*, Refs. 58–61. Furthermore, lower alcohols are compatible with PDMS.[23] By controlling the reflux, catalysis and hydrolysis conditions, the nature of the resulting solution precursors and gels can be controlled. An advantage of $Si(OR)_4$ and silsesquioxane $R'Si(OR)_3$-based sols is that they can be made in a relatively stable form even at high solids concentrations. This minimizes shrinkage upon gelation. And since no crystallization or precipitation occurs, the replicated pattern shapes can be retained more easily.

Similar formulations can also be made using non-silicon alkoxides, *e.g.*, $Ta(OC_2H_5)_5$,[62] $SnCl_2$,[63] and $Ti(OC_2H_5)_4$,[64] in ethanol or 1-propanol. However, the details of the chemistry of hydrolysis and condensation are different since the reactions are thermodynamically rather than kinetically controlled,[57] and precipitation will eventually occur upon drying.

Many synthetic approaches start from short-chain carboxylate precursors dissolved in carboxylic acid, *e.g.*, $M(CH_3COO)_n$ in acetic acid, and metal alkoxides.[55] The carboxylic acid serves both as solvent and as chelating stabilizer for the very reactive metal alkoxides, and some exchange of ligands takes place after mixing. In this way precursor formulations for $Pb(Zr,Ti)O_3$ (PZT)[65] and $BaTiO_3$ (BTO)[63] have been prepared. During drying, they react with water to form condensed structures. Also the formation of ZnO from $Zn(CH_3COO)_2$ and water is an example of such a process.[63]

Metal–organic decomposition (MOD). In this approach metal carboxylates and acetates with long-chain ligands are dissolved in a common unreactive solvent, usually xylene.[55] Since the starting compounds are insensitive to water, the metal organic solutions are essentially simple mixtures of the starting compounds. The inorganic phase is only accomplished in the final thermal treatment step after patterning and drying. The precursor formulation has a low surface energy, but a serious disadvantage of xylene as a solvent is the high degree of swelling that PDMS

undergoes when it is exposed to non-polar solvents.[23] MOD synthesis has been employed to pattern several complex oxides, *e.g.*, epitaxial $SrBi_2Ta_2O_9$ (SBT)[66] and PZT.[67]

Chemical bath decomposition (CBD). This synthesis route is used to grow solid films from solution by single or repeated immersions of a substrate in a bath. Usually pH, temperature and/or composition of the source solution are adjusted.[56] When prepatterned substrates are employed, site-selective nucleation and growth may occur, as will be discussed in more detail in Section 4.2. This approach has been explored in particular by the group of Koumoto at Nagoya University.[14] A typical example is the formation of titania from $(NH_4)_2TiF_6$ and H_3BO_3[68]:

$$TiF_6^{2-} + 2H_2O \rightarrow TiO_2 + 4H^+ + 6F^-$$

$$BO_3^{3-} + 4F^- + 6H^+ \rightarrow BF_4^- + 3H_2O$$

The second reaction scavenges the produced fluoride and is used to control the rate of titania formation.[69] The bath solutions are usually very dilute, so they are not commonly used in moulding-based processes.

Nitrate route. This route has been used in soft lithography by few researchers.[70,71] Essentially, the precursor solution is made by simply dissolving metal nitrates. To avoid substrate dewetting and recrystallisation phenomena during drying of the precursor, metal-coordinating polymers such as poly(acrylic acid) can be added to the solution.[70]

Suspensions. Suspensions are employed in particular in those cases in which relatively large dimensions, and/or patterns with high-aspect ratios are targeted.[72,73] The volume fraction of solids in suspensions can be raised to higher values than is possible with the solution-based approaches described above. Moreover, although the relative degree of shrinkage of a precursor solution upon drying and consolidation may be independent of the actual size of the feature that is formed, absolute shrinkage scales with object size. This is why high-aspect ratio objects with dimensions above 10–20 μm are best made from suspension-based precursors. The successful use of suspensions with solids volume concentrations up to 40 vol% and reasonable viscosities has been reported.[73]

The four key physical properties of precursor solutions and suspensions are:

1. Solids content (or equivalent). High solids contents are favourable since the metal concentration is related to the solids volume in the final oxide. Shrinkage upon drying and thermal after-treatment is suppressed when the solids content is increased. For instance, the quality of shape replication in moulding-based processes is improved when the metal concentration in the precursor is increased.[73]
2. Viscosity and rheology. In MIMIC, low viscosities are needed in order to enable fast penetration of the precursor into the micropatterned channels.[73] This implies a high solvent concentration and low solids content. If necessary, raising the temperature during patterning may help to decrease the viscosity of the precursor further.[74] The shear rate dependence of viscosity is particularly important when non-Newtonian fluids are applied in MIMIC, since the rate of penetration is not constant during the patterning process.[73]
3. Surface energy. The surface tension of precursor solutions determines the wetting interaction of the ink in the mould, as will be discussed in more detail in Sections 2.4 and 3. Low surface tension promotes wetting of a relief-patterned stamp and is required when water-based solutions are employed, but good wetting may hamper the debonding step in which stamp and ink are separated.[75]
4. Types of solvents. The concentration and volatility of solvents determines the drying rate and drying time. Faster evaporation will lead to faster solidification of a precursor, and increase the throughput that can be accomplished in industrial processes. On the other hand, it has also been shown that the packing efficiency of particle-based suspensions is improved when the drying process inside the channels proceeds slower.[76] Alternative ways to slow down the drying rate are soaking of the mould in the solvent prior to use, and/or drying in atmospheres in which solvent vapour is already present. Solvent types also determine the degree of swelling of the elastomeric mould.[23]

2.4. Wetting, demoulding, and thermal after-treatment

Optimal wetting of microchannels by fluids is an important factor in moulding-based approaches. A rich variety of mechanically stable, metastable, and unstable liquid morphologies can be found,[77,78] depending on (i) the contact angle between fluid and surface, and (ii) the geometric details (aspect ratio) of the grooves.

Obviously, a very large contact angle (>90°) indicates that the interfacial energy between ink and mould is rather unfavourable. This promotes the dewetting (debonding) of the grooves of a mould, in particular when the height-to-width aspect ratio of the structure is smaller than 0.5. When the aspect ratio is higher, even fluids with a very large contact angle can fill microchannels in a thermodynamically stable way. Small contact angle fluids fill the channels spontaneously,[78] but release from the mould after patterning may be problematic.[75] When the contact angle is smaller than 45°, wedge wetting may occur, a thermodynamically stable mode of filling in which only the corner edges of a channel are filled with fluid.[78] The special feature of wedge wetting is that feature sizes can be printed that are much smaller than the resolution of the mould. In order to print (polymeric) patterns that resemble the shape of the stamp, one should work in a wetting regime where the liquid forms elongated channels with negligible Laplace pressure.[77]

It has been shown theoretically that relatively large contact angles between mould and precursor solution are required to facilitate debonding after moulding-based patterning, ideally >90°,[75] see Fig. 2. Under such conditions the energy released per unit area of crack (debonding) extension, is very large for small cracks. This promotes the release of dried precursor from the mould. For contact angles smaller than 90°, the driving energy for crack propagation is rather small and concave surfaces effectively inhibit debonding.

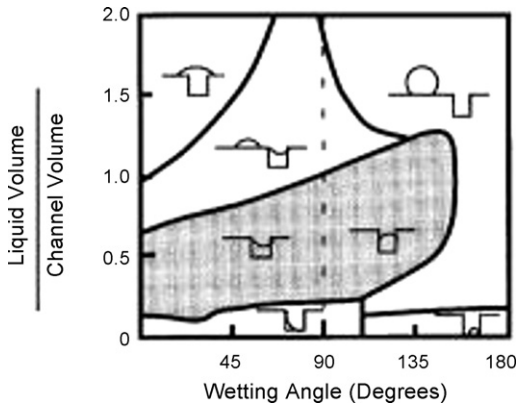

Fig. 2. Equilibrium configurations of a liquid on a channelled stamp. The ratio of liquid volume over channel volume is plotted versus contact angle of the liquid. The grey area represents the conditions in which channel filling is stable. Reprinted with permission from Ref. 75. Copyright 1999, American Institute of Physics.

Most of the formed patterns require a post-patterning heat treatment step to convert the dried precursor into the desired crystalline phase, remove residual organics and densify the thin film. Due to the small sizes of the features to be sintered, relatively low sintering temperatures and short sintering times are sufficient. Shrinkage presents a serious technical problem in ceramics processing in general and in the micro- and nanopatterning of ceramics in particular, since it limits the quality of pattern replication. An overall shrinkage of 80–95% is common for many of the reported chemistries.[65,70] For many applications this may not present a problem. However, when more complex, hierarchical patterns are to be realized, factors like 3D topography, shape replication fidelity, and edge sharpness become crucial factors to consider.[38,79]

Cracking may present a problem, but micropatterned ceramics are able to release mechanical stresses in both the vertical direction and lateral direction, and this helps to form higher structures than would be possible in the case of continuous thin films.

It has been shown that there are limits to submicrometer resolution patterning of macromolecular fluids and low molecular weight polymer because of the Rayleigh instability.[46] The Rayleigh instability is primarily a geometrical effect, and becomes relevant for pattern transfer in the 100–1000 nm range. Where precursor solutions and suspensions are concerned, the extent to which this effect can play a role depends on the rate at which the precursor solution dries physically via evaporation of solvents, and/or condenses chemically into a higher molecular weight network.

3. Moulding-based patterning techniques

3.1. Microtransfer moulding (μTM)

Microtransfer moulding has not been explored widely for the formation of metal oxide patterns, which is somewhat surprising considering its speed, ease of patterning isolated features, and ability to pattern on non-planar substrates. The concept of microtransfer moulding was introduced by Zhao, Xia, and Whitesides in 1996 and demonstrated for several polymers and spin-on glasses.[8] From a simple model it can be concluded that the following general condition should be fulfilled in order to both pattern and demould line features[80]:

$$\gamma_{\mathrm{sol}} < \gamma_{\mathrm{mould}} < (2a+1)^{-1}\gamma_{\mathrm{substrate}}, \quad (1)$$

where a is the aspect ratio of the line structure, and γ_{sol}, γ_{mould} and $\gamma_{\mathrm{substrate}}$ are the surface energies of liquid precursor solution, mould, and substrate on which the pattern is formed, respectively.

Lange and co-workers described the epitaxial patterning of 500 nm wide lines of ZrO_2 on single crystal cubic zirconia, and the epitaxial patterning of 50 μm wide lines of $SrBi_2Ta_2O_9$ (SBT).[66,75] Metal–organic decomposition (MOD) solutions of metal (Sr,Bi,Zr) 2-ethylhexanoates and tantalum ethoxide in xylene were spin-cast onto a patterned PDMS mould, and transferred to the substrate. In the case of SBT, it was shown that the oxide had a (0 0 l) out-of-plane orientation after thermal processing, and a single in-plane orientation on (0 0 1) $SrTiO_3$. Microtransfer moulded patterns have also been reported in a few other cases, *i.e.*, mesostructured mesoporous silica lines of 1–3 μm width and 1–2 μm height with a low refractive index (1.15) for waveguide arrays.[81] Nanotransfer molding with elastomeric PDMS moulds has been demonstrated for PZT line and pit patterns with lateral resolutions down to 100 nm, and a feature height of ∼25 nm after thermal treatment.[80]

Patterns with much higher aspect ratios can also be made by microtransfer moulding, *i.e.*, for the fabrication of ceramic microcomponents for microelectromechanical systems (MEMS).[72,82–84] Such components are typically in the millimetre size range, they contain features of 30–100 μm, and have high-aspect ratios of up to 10. Because of their large sizes it is of the utmost importance to minimize shrinkage upon drying and thermal post-treatment. Concentrated ceramic suspensions of α-alumina with up to 80–84 wt% solids were therefore used, with added dispersants. Smaller features in the micron range would be possible if finer particles with 0.1–0.2 μm would be used, but these also suffer more from shrinkage.[85] It is important to form the feature directly in its final form, since post-processing such as grinding and polishing are difficult, especially on the scale of the feature sizes. Due to the high viscosity of the used suspensions, centrifugal casting has been introduced to improve the filling of the PDMS mould, and thereby the densification of the green bodies within the moulds. This process has been termed centrifugally aided soft moulding (CASM).[84]

3.2. Micromoulding (embossing)

Micromoulding is much more commonly used for patterning oxides than transfer moulding. All-printed all-inorganic transistors, photodetectors, resistors, and multilayer structures with sacrificial layers and vias have been made.[86] An advantage of micromoulding is that less stringent conditions apply to the wetting properties of the precursor solution or dispersion with respect to the mould than in microtransfer moulding.

Nonetheless, Marzolin et al. pointed out that the liquid should spontaneously dewet the elastomer surface so that the protruding parts of the mould make conformal contact with the substrate, and thus avoid a residual layer.[60] The dewetting process is driven by both the applied pressure and the differences in interfacial tensions, *i.e.*, substrate–elastomer γ_{SE}, substrate–liquid γ_{SL}, and liquid–elastomer γ_{LE}. The dewetting speed is proportional to S, where

$$S = \gamma_{SL} + \gamma_{LE} - \gamma_{SE}. \quad (2)$$

Since γ_{LE} is more or less fixed, the solution can be optimized by adding low viscosity solvents with a high surface tension which do not swell the mould.[60] Residual layers are very hard to be avoided.[87] For applications in which merely a patterned surface is needed, this may not present an important issue. However, when isolated features are required, an etching step or another equivalent method to remove residual material between the patterned features will be necessary. The reported studies fall roughly in two categories: (a) namely silica glasses and silicate–organic hybrid materials for optical and dielectric applications, and (b) non-silicon based functional metal oxide materials, *e.g.*, ferroelectrics and electrically insulating materials. These will be discussed separately below.

1. *Glasses and hybrids for optics and dielectrics*

The first papers date back to 1988[58] and precede the soft lithography era which started in 1993.[7] Tohge et al.[58] reported the fine patterning of sol–gel derived boron-doped silica on glass substrates. Features with a width of 1.2 μm and thicknesses of 100–300 nm after thermal treatment were made. The nature of the rigid mould was not mentioned.

Optical waveguiding applications typically require thicker patterns, in the order of one micrometer. Alternative materials were proposed to meet this criterion, such as organically modified ceramic (ORMOCER) from a precursor mixture of methacryloxypropyl trimethoxy silane, methacrylic acid, and zirconium alkoxide.[59] ORMOCERs have a lower elastic modulus and are more ductile than inorganics, so shaping the precursor into the mould is easier, while cracking occurs less easily during the embossing step. Square array and line patterns after UV curing had lateral dimensions of 10 μm and a thickness of no less than ∼3 μm. The aspect ratio of about 0.3 is still quite modest.

Soft-lithographic patterning of sol–gel solutions using PDMS was first demonstrated by Marzolin et al.[60] They employed a tetramethylorthosilicate-based solution, an elastomeric mould with micrometer-sized features, and applied a pressure onto the mould of about 0.7 bar during the process. Glassy titanosilicate (Ti/Si = 0.07) membranes, and aluminosilicate (Al/Si = 0.09) and borosilicate (B/Si = 0.1) line patterns with waveguiding capacity were formed following the same approach. When sol–gel derived organic–inorganic hybrid materials such as silsesquioxanes and organosilanes are applied to the micromoulding technique instead of glass precursors, the hardness and shrinkage can be optimised by adjusting the type and amount of organic groups. Mixed sol–gel solutions of ($MeSiO_{3/2}$)–(SiO_2)[88] and ($MeSiO_{3/2}$)–(C_6H_5–Si–$O_{3/2}$)[79] on glass can replicate the features of a mould nearly perfectly with minimal shrinkage (∼4%), provided that a hard mould is used. Moreover, optical properties like transmittance and refractive index can be controlled through proper selection of the organic groups, which is why these materials are so popular for these applications.[89] A comparison between soft lithographically produced photonic crystal laser resonators from epoxide- and methyl-functional organosilanes, and photolithographically fabricated resonators in silicon showed that the laser emission spectra were of equal quality.[90] Patterned features were ∼500 nm in width and ∼50 nm in depth, and could be solidified at 60 °C.

Closely related sol–gel processed organosilicas have been studied for use in interlayer dielectric (ILD) insulator films. The low dielectric constant $k < 2.3$ that is required in next generation ILDs to suppress cross-talk between neighbouring interconnect lines and minimize power dissipation can only be realized by introducing large-scale nanoporosity. Other requirements are an elastic modulus $E > 6$ GPa, and a low thermal expansion coefficient TEC $< 30 \times 10^{-6}$ °C^{-1}. Ro et al. demonstrated nanoporous poly(methylsilsesquioxane)-based patterns that meet all these requirements.[91] Nanoporosity was introduced into the patterned material by incorporating a poly(ethylene oxide)-*b*-poly(propylene oxide) copolymer amphiphile in the liquid precursor, a concept that was originally introduced by Yang et al.[92] The surfactant was burnt out in the final thermal treatment step. The porosity was ∼20%.[91] The mould was a rigid silicon oxide line gratings structure with 100 nm width and 170 nm height, with a pitch of 200 nm. During imprinting, pressures up to 34 bar, and temperatures up to 200 °C were applied, and the features of the mould could be replicated with high fidelity. Only modest shrinkage occurred, mainly in the vertical direction. In a later study[93] the same group showed that decreasing the block copolymer porogen concentration in the solution led to lower levels of mesoporosity (pore size >2 nm), but a substantial degree of microporosity (pore size ≪2 nm) remained. The net effect was a decreased interconnectivity in the pore network, which is beneficial for electrical insulation. Moreover, it was shown that a dense skin formed over the patterns during the process. The skin can protect the porous ILD structure from reactive sources of contamination in subsequent processing steps.

Researchers from Philips Research demonstrated a soft imprinting technique with which they fabricated a 3D photonic woodpile structure made of sol–gel silica.[94] They employed a PDMS mould and used a combination of gravity and capillary force to imprint the mould into the wet layer. No external pressure was applied. In this way the distortion of the mould could be kept smaller than 0.03% over an area of 15 mm × 15 mm. They imprinted a pre-dried 88 wt% methylsilsesquioxane-silica (1:1 molar ratio) thin film. The high solids content ensured minimal shrinkage (∼7%) during drying, and good shape replication of the square woodpile structures of 70 mm × 65 nm, which is crucial for making photonic crystals. After deposition of each line pattern, the empty volume between the lines was filled with polystyrene to planarize the layer for deposition of the

Table 2
Surface tension of imprinting materials and the adhesive force of the PDMS mould to each material. Table adopted from Ref. 98.

Imprinting materials	Surface tension (mN/m)	Adhesive force (mN)	Adhesive force/unit area (nN/nm^2)
Fluorinated methacryl hybrimer[98]	15.9–22.3	0.78–0.88	0.138–0.156
Methacryl hybrimer[95]	28	2.45	0.435
Perfluorocyclobutane	22.6	1.15	0.204
Tri(propylene glycol) diacrylate	30.3	2.5	0.43
PMMA	41.1	6.5	1.16

next line grating. As polystyrene dewets the upper surface of the hydrophobic silica grating at elevated temperatures, a completely planar layer could be accomplished by exactly dosing of the amount of polystyrene to fill all voids between the woodpiles, and raising the temperature to 150 °C. Four layers were realized. Residual layers (~15 nm thick) after imprinting were removed with a short acid etch.

Solvent-free thermally curable epoxy-terminated siloxane prepolymers for low pressure NIL have also been developed.[37] A suitable prepolymer for this process should have a low viscosity at room temperature, while curing time and temperature should be minimal. As the process is solvent-free, shrinkage is minimal, and the time of solidification is short. The final polymer should be rigid to avoid deformation and exhibit good adhesion to different substrates (silicon, silica, GaAs, organic films), and the chemical structure of the polymer should allow for wet etching in organic solvents or aqueous solutions. The viscosity of the reported prepolymer was <10 mPa s at room temperature, and by stoichiometric reaction with diamines it was transformed into an epoxy-amine network. Line patterns of 60 nm width, 80 nm height, with a residual layer less than 20 nm thick were demonstrated. Imprinting even smaller features resulted in line deformation and collapse. An alternative solvent-free route to UV curable high refractive index organic–inorganic hybrids with both hydroxyl and vinyl functional groups has also been reported.[95] These materials were applied as imprint resist in NIL on 100–300 nm length scale. Polysiloxane prepolymers were made by non-hydrolytic alkoxylation of 3-(trimethoxysilyl)propyl methacrylate, diphenylsilanediol,[95] and titanium ethoxide[61] precursors, using $Ba(OH)_2{\cdot}xH_2O$ as basic catalyst. The viscosity of the prepolymer was controlled between 20 and 220 mPa s,[96] so that little pressure was required to imprint a pattern. Imprinted layers were made using patterned PDMS, followed by low energy UV cross-linking of the reactive vinyl groups.[61,97] Since PDMS is transparent, the pattern can be UV cured through the PDMS mould. Typical curing times were 30 s, using 365 nm UV light.[61,98] It was shown that the refractive index of the hybrid material could be tuned between 1.47 and 1.53 to meet the requirements for waveguiding and photonic crystal applications.

A fluorinated version of the material with a relatively high *E*-modulus of 40 MPa, low surface tension, low shrinkage, and high etching resistance was also developed.[38,96] It has been tried out as imprint resist,[99] but since the viscosity of the fluorinated prepolymer was rather high, it left a rather thick residual layer. The material is more interesting to be applied in nanopatterned moulds for imprinting other materials.[96] The adhesive strength is low, substantially lower than non-fluorinated hybrids and even lower than perfluorocyclobutane, see Table 2.[98] The flexibility of this so-called fluorinated hybrimer is lower than that of PDMS, which complicates achieving good conformal contact between mould and substrate. The prepolymer was therefore mixed with acrylate monomers to increase the flexibility of the resulting mould material. Alternatively, to make the material suitable for application as imprint resist, *tert*-butyl acrylate was added to the prepolymer to lower its viscosity.[38] Feature sizes as small as 40 nm with perfect replication of the shape of the mould were fabricated, as illustrated in Fig. 3.

Titania films with a high density of high-aspect ratio pores or pits perpendicular to the surface, and a diameter of 35–65 nm were made by imprinting a sol–gel titania with a hard PMMA mould and a soft PDMS mould that consisted of irregular arrays of rods.[64] The aspect ratios were 2–3. PDMS did not work well due to its low Young's modulus.

2. *Functional metal oxides*

The fabrication of complex three-dimensional lead zirconate titanate ($PbZr_xTi_{1-x}O_3$; PZT) micropatterns with 10–150 μm features and aspect ratios of 3–10 for microelectromechanical systems (MEMS) has been demonstrated using a lost mould method.[72,82] PZT powder and an organic binder were calendered into a viscous polymer processed ceramic tape, which was subsequently embossed by a mould at 10 MPa. After drying the tape the PMMA mould was dissolved in acetone or chloroform. The remaining left-over composite patterns were then calcined and

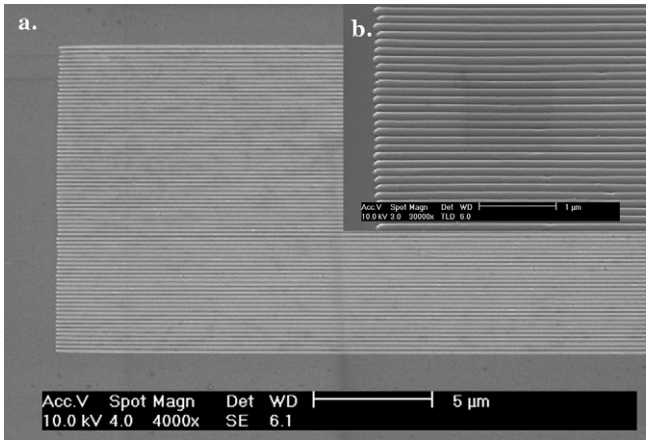

Fig. 3. (a and b) Imprinted line pattern on fluorinated resist with a line width of 40 nm using a modified flexible fluorinated hybrimer mould. Reprinted with permission from Ref. 38. Copyright 2006 Institute of Physics.

sintered into solid PZT. Removal of the mould without damaging the green structure was found to be difficult when feature sizes were below 100 μm and aspect ratios >3 were targeted.

Nanopatterned arrays of PZT with 200–350 nm resolution have been made by imprinting sol–gel and MOD-based precursor films with a hard silicon mould[67,80,100] and soft PDMS.[80] To maintain the shape of the imprinted pattern it is necessary that the grain size after annealing is at least an order of magnitude smaller than the feature size of the pattern. In practice the MOD-based imprinted patterns were found to have grains of 250 nm, close to the feature size, while the sol–gel based pattern has grains of 35 nm at a pattern height of ~50 nm. Loss of lead during annealing is an increasingly important issue in PZT nanostructure fabrication as the surface-to-volume ratio increases. In this study lead loss seemed to depend on the chemistry of the system, being more serious for MOD patterns than for sol–gel based patterns.

It has also been shown possible to pattern ferroelectric $PbTiO_3$ phase in lines and dots of 700–1000 nm width on $SrTiO_3$(0 0 1), with the $PbTiO_3$ grown epitaxially.[70] However, the shrinkage during drying and thermal after-treatment is in all cases very high. For example, ZnO and Al_2O_3 patterns that were embossed from poly(acrylic acid) (PAA)-based polymeric metal nitrate solutions typically exhibited a shrinkage of 80% or more.[70,87] Non-patterned continuous films shrunk only in the vertical direction, because of the constraint imposed by the substrate. Patterned films also showed lateral shrinkage by 40–90%, depending on the nature of the substrate and/or the patterned material. Imprinting a PZT/Au bi-layer film in a single imprinting step is nonetheless feasible, as illustrated in Fig. 4.[101,102] In comparison with a single-layer PZT film, the profile in the bi-layer PZT/Au was much deeper and clearer. Apparently the soft gold cover layer helps to shape the PZT film.

Sub-500 nm structures of various sol–gel derived functional oxides (TiO_2, SnO_2, ZnO, $In_xSn_{1-x}O_2$ (ITO) and $BaTiO_3$) with high-aspect ratios were recently demonstrated by using a perfluoropolyether (PFPE) elastomer as mould material.[63] PFPE has a very low surface energy ($\gamma \ll 20$ mJ/m^2), is permeable to gas, and chemically inert to most solvents. The gas permeability of the moulds allowed complete filling by the precursor, and drying of the embossed film. Nanoscale arrays with features of ~200 nm width, and aspect ratios up to 2.5 over mm-scale areas were realized.

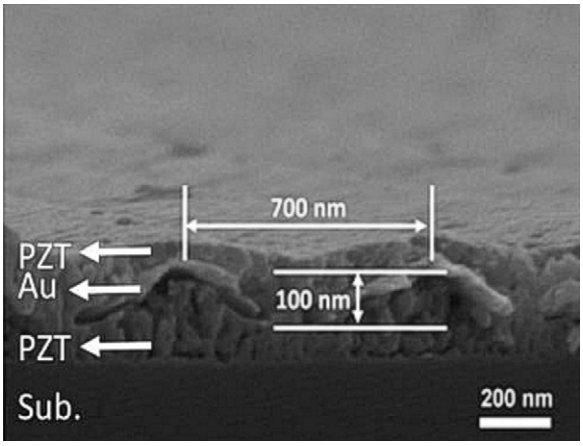

Fig. 4. Electron microscope image of a PZT/Au/PZT nanoimprinted structure after sintering. Reprinted with permission from Ref. 102. Copyright 2008 Institute of Physics.

Nanometer-scale titania features have also been made with conventional micrometer-scale patterned elastomers by exploiting the edge topography of the elastomer-substrate corner.[103] Essentially, a conventional PDMS mould was imprinted ($p \sim 0.08$ bar) into a wet film of dilute sol, after which the film is dried while the mold was held in place. The capillary force drove the solution to form menisci between the stamp protrusions. At the same time, the solution moved to the edges of the stamp protrusions due to capillary flow, which resulted in isolated structures smaller than the lateral spacing of the stamp's protrusions. The dimensions could be controlled by setting the concentration of the solution, the duration of solvent evaporation, and the temperature. It may provide a facile route for fabricating large area patterns of metal oxide. The same strategy, *i.e.*, exploiting the thermodynamically favourable confinement of the corner region to fabricate inorganic or hybrid structures with features smaller than the protrusions of the stamp, has also been demonstrated in a somewhat related gas phase process,[104] as discussed in the next section.

A variation to conventional micromoulding was proposed and elaborated by the Gauckler group from ETH Zurich. Instead of moulding a ceramic relief pattern on a flat substrate, Schönholzer et al.[85,105] cast colloidal alumina suspensions onto prepatterned substrates. Photoresist patterned silicon substrates were employed.[85] Defect-free ceramic replicas of alumina, zirconia, Gd-doped CeO_2, and tin oxide with a pattern resolution of ~1 μm and aspect ratio below 1 after sintering were accomplished in hydrophobic moulds.[105] Hydrophilic moulds suffered from too much adhesion between mould and ceramic, resulting in defect formation during the demoulding step. The same approach has been employed later by others with different types of precursor solutions and patterned substrates, in a number of cases aimed at the fabrication of stand-alone ceramic micropatterns and nanopatterns.[106,107] Examples are the fabrication of sol–gel titania nanowires on a groove patterned polymer,[106] AlN by reactive sputtering on micropatterned noble metal substrates,[108] PZT micro-cantilevers in silicon,[107] titania and graded titania-iron oxide nanorod arrays with 120 nm features by CBD on prepatterned silicon and bioden acetate substrates,[109,110] and titania gratings and arrays on indium tin oxide.[111]

A relatively recent nanoscale moulding-like technique was proposed by Dravid and co-workers.[112] After creating a 3D patterned polymer-based resist film on a hard substrate using soft e-beam lithography, all formed voids in the resist film were filled with a spin-on sol–gel precursor, followed by removal of the resist and consolidation of the sol–gel. In this manner functional patterns of ZnO,[113] $BiFeO_3$,[114,115] $BaTiO_3$,[116,117] and $CoFe_2O_4$[117] with resolutions down to 40 nm were made. The method illustrates how small the features are that can be realised with sol–gel chemistry. Although e-beam lithography is strictly speaking a serial patterning approach, similar

objects and patterns would also have formed when a parallel prepatterning technique had been used to make the bas-relief pattern.

3.3. Micromoulding in capillaries (MIMIC)

The concept of micromoulding in capillaries was proposed by the Whitesides group in 1996.[27] Along with a number of polymers, they demonstrated it for a low viscosity spin-on glass, poly(ethoxymethylsiloxane), which was converted into silica by pyrolysis at 400 °C in air. The obvious advantage of MIMIC in comparison with micromoulding and microtransfer moulding is that the mould is dry when it is placed on and makes conformal contact with the substrate. Residual layers are therefore avoided. Hence, MIMIC could contribute to an all-additive fabrication scheme, excluding subtractive etching steps to remove undesired material. The applicability of the method has been illustrated by the fabrication of a tin oxide based microsensor,[118] and patterned etch resists in the fabrication of silicon MOSFETs (Metal Oxide Semiconductor Field Effect Transistors).[119] The latter study demonstrated the compatibility of MIMIC with Si fabrication processes.

Possible disadvantages of MIMIC are that (i) it is a quasi-parallel patterning technique with an inherently lower rate than true parallel patterning processes, (ii) the formation of isolated features is impossible, and (iii) the precursor viscosity should be low in order to ensure acceptable filling rates. The rate of infiltration of the precursor into the channel decreases as the length of the capillary increases. For a tubular channel with a hydraulic radius R, the rate of penetration dz/dt is expressed by the Washburn equation[120]:

$$\frac{dz}{dt} = \frac{R\gamma_{LV}\cos\theta}{4\eta z} = \frac{R(\gamma_{SV}-\gamma_{SL})}{4\eta z}. \quad (3)$$

Here z is the length of the liquid capillary inside the channel, η is the viscosity of the penetrating liquid, R is the ratio between capillary volume and the surface area of the channel, and θ is the contact angle of the fluid meniscus inside the capillary. The surface tensions γ_{LV}, γ_{SV} and γ_{SL} are the surface tensions between liquid and air, channel wall and air, and channel wall and liquid, respectively. It follows after integration that

$$z(t) = \sqrt{\frac{R(\gamma_{SV}-\gamma_{SL})t}{2\eta}}. \quad (4)$$

The equation shows that although the capillary force of a channel increases with decreasing hydraulic radius R, this effect is more than counterbalanced by the increased friction exerted by the channel walls, so filling rates are lower in smaller channels. A generally applicable method to increase the filling rate is to reduce the viscosity of the precursor solution by increasing the temperature during the MIMIC process,[74] but it has not been exploited for patterning ceramics to date.

The main driving force for MIMIC is the free energy change ΔG upon filling the channel with a fluid. For a square channel with width and height a, the free energy gain can be approximated by[120]

$$\Delta G(t) = -az(t)\gamma_{LV}(3\cos\theta_{mould} + \cos\theta_{substrate}), \quad (5)$$

where θ_{mould} and $\theta_{substrate}$ are the contact angles of the liquid with the surfaces of the mould and the substrate, respectively. Detailed modelling and experimental studies have been reported by Huang, Liu, and Li.[121] For a hypothetical square channel with different contact angles θ_1, θ_2, θ_3, θ_4 for each of the surface walls, the equivalent contact angle θ can be expressed as

$$\cos\theta = \frac{1}{4}(\cos\theta_1 + \cos\theta_2 + \cos\theta_3 + \cos\theta_4). \quad (6)$$

The pressure drop Δp_{LV} over the meniscus of the capillary front for a square channel with sides a is given by[121]:

$$\Delta p_{LV} = \frac{4\gamma_{LV}\cos\theta}{a}. \quad (7)$$

Hence, when the equivalent contact angle in Eq. (7) is smaller than 90°, spontaneous penetration into the channel occurs because of the positive pressure drop. Although penetration should be theoretically possible even in very narrow channels, numerical analyses and experimental evidence showed that surface tension can affect the filling rate in a negative manner to such an extent that even pore blockage can occur near the exits of very small channels.[122] Optionally, the driving force for liquid penetration could be increased by 1 bar by generating a low vacuum in front of the penetrating liquid.[123]

The shape of the imbibition front of liquid precursors has been studied in detail.[120,121] Depending on the surface energy of the channel wall γ_{SV}, different spreading regimes can be observed, as illustrated in Fig. 5. Liquids penetrating a channel with walls of low surface energy show capillary fronts that advance as a whole. But as the surface energy of the channel increases, precursor structures advancing in front of the macroscopic body of liquid are observed, especially in the corners between mould and substrate. Some of these structures include slipping films and shoulders. Similar regimes have been observed with differences in the velocity of imbibition on surfaces of constant γ_{SV}.[120] The thermodynamics of wetting on patterned surfaces has been studied in detail by Seemann et al.,[77,78] as discussed in Section 2.4. Modelling of the dynamics for penetrating liquids

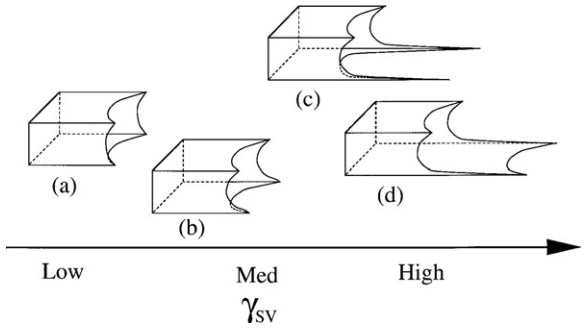

Fig. 5. Schematic summary of different spreading regimes observed in MIMIC. Shapes of the penetrating liquids in PDMS capillaries are formed on (a) SAMs with low γ_{SV}, (b and c) SAMs with medium γ_{SV}, and (d) SAMs with high γ_{SV}. Reprinted with permission from Ref. 120. Copyright 1997 American Chemical Society.

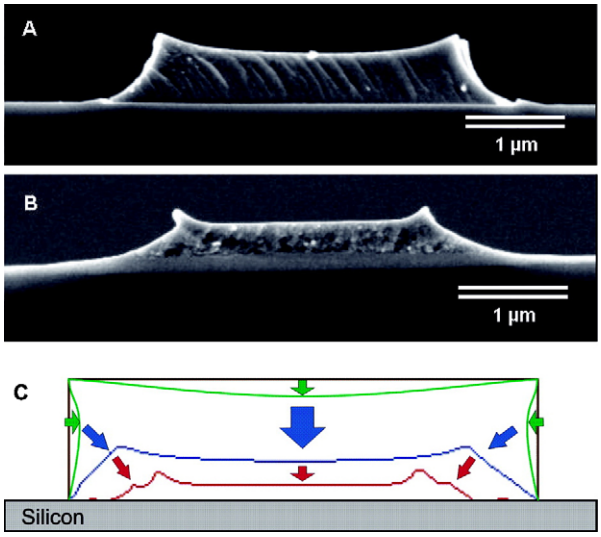

Fig. 6. SEM images of a cross-sectioned 5 μm wide sintered PZT line on Si patterned from a 1.85-μm depth PDMS mould (a) after drying and (b) after heat treatment and (c) a schematic diagram of the drying process leading to peak formation. Reprinted with permission from Ref. 65. Copyright 2003 American Chemical Society.

that have varying advancing contact angles with different walls of the channel indicate that a rich variety of capillary front shapes are possible.[121]

The typical non-uniform cross-sectional topography, illustrated in Fig. 6 for patterned sol–gel PZT lines after drying and consolidation, was observed in several other studies.[65,124,125] The film thickness is greater near the lateral edges than in the middle. The phenomenon can be explained by preferential wetting of the gel to the corners of the PDMS mould, and subsequent locking-in of the structure by accelerated drying rates at the corners. The double peak profiles were less prominent and had a higher density when the patterns dried more slowly.[65]

Quite a number of functional materials have been patterned using MIMIC, in most cases by employing low viscosity sol–gel precursor solutions. In the 1–10 μm lateral resolution scale, functional oxide micropatterns of SnO_2 and ZrO_2,[124] PZT and $Sr_2Nb_2O_7$,[125,126] and $La_{0.7}Sr_{0.3}MnO_3$[71] have been reported. Several luminescent materials have been patterned, *i.e.*, the green luminescent layered perovskite-type hybrid $PbI_4(C_6H_5C_2H_4NH_3)_2$ (resolution 0.8–50 μm),[127] YVO_4:A (A = Eu^{3+}, Dy^{3+}, Sm^{3+}, Er^{3+}),[128] $La_{9.33}(SiO_6)_4O_2$:A (A = Eu^{3+}, Tb^{3+}, Ce^{3+}),[129] Y_2O_3:Eu^{3+},[130] A_2SiO_5 (A = Eu^{3+}, Tb^{3+}, Ce^{3+})[131] and Rhodamine B doped epoxy-functional organosilica[132] have been made. Also non-oxide ceramics SiC[133] and SiCN[134] have been patterned using MIMIC.

Trau et al. applied a strong electrical field tangentially to the surface within the capillaries, so that an additional electroosmotic flow force was induced to increase and maintain the flow rate of the precursor.[135] Under these conditions, the viscous forces within the flowing solution were able to align tubular cetyl-trimethyl ammonium chloride surfactant micelles present in the solution parallel to the channel wall. In combination with the ongoing gelation of a silica sol, this resulted in silica micropatterns with an internally oriented mesostructure.[135] In subsequent work, block copolymer templating of silica to fabricate patterned mesoporous optical waveguides,[81,136] and the incorporation of close-packed 200–2000 nm polystyrene spheres into silica to make patterned photonic crystals[137] have been reported. Recently, Kim et al. developed photocurable 20 μm thick organosilica micropatterns for the immobilization of proteins.[138] The sol–gel hybrid had amine and methacryl functionalities for covalent linking with proteins and photocuring, respectively. Because the amine functionality is incorporated in all siloxane oligomers, immobilizing sites for proteins such as streptavidin are widely distributed over the surface of the material.

Organosilane patterns with nanometer lateral resolution have been made using a MIMIC-like gas phase deposition process using PDMS stamps with micrometer-scale features.[104] The stamps were placed in contact with a silicon substrate, after which the system was exposed to low pressure 3-aminopropyl triethoxysilane (APTES) vapour ($p \sim 10^{-5}$ bar). The precursor condensed selectively along the PDMS-substrate corner lines in the early stages of the process, to form 200 nm wide line patterns with a height of ~7 nm after 3 h of exposure. Long-term exposure led to condensation of APTES on the entire surface, and reduced the lateral resolution of the formed patterns to that of the stamp. The organosilane precursors used for forming such structures can also be supplied by spontaneous release from a preloaded PDMS stamp.[139] Both these methods bear resemblances with another study discussed elsewhere in this review.[103]

An application for suspension-based MIMIC has been demonstrated by the fabrication of a tin oxide gas sensor covering an area of only 10 μm × 40 μm, about 2 orders of magnitude smaller than commonly used today.[118] The sensor device shown in Fig. 7 included a heating element to increase sensitivity and response times, and Pt electrodes to measure resistance (changes) in the MIMIC-patterned SnO_2 lines when exposed to different gas mixtures. The tin oxide colloidal suspension containing 33 vol% solids was optimized for a low viscosity of 25 mPa s at a shear rate of 100 s^{-1}. Nanoparticle solutions and colloidal suspensions with a d_{50} of 280 nm were employed.[140,141] Although the penetration rates are higher when low viscosity solutions (<200 mPa s) and low solids loading (<5 vol%) are employed,[142] more concentrated suspensions can also be used, albeit that the penetration length of the suspensions becomes shorter as the viscosity increases.[73] However, the main advantage of higher concentrated suspensions was that higher aspect ratios, up to ~1 for 33–40 vol% SnO_2, could be accomplished.[73] The pattern after sintering consisted of 10 μm wide and 5 μm high lines of 1.0 mm length. The final lines were bell-shaped. No double peak profile[65] occurs here, since no gelation but only physical drying occurred. A practical limitation of MIMIC when applied to suspensions or sol–gels is the considerable degree of volumetric shrinkage that results from drying and thermal after-treatment. In an attempt to overcome this problem for suspensions, Imasu and Sakka recently demonstrated the possibility to form very densely packed beds of powder using low solids suspensions (~5 vol%) and MIMIC. A requirement

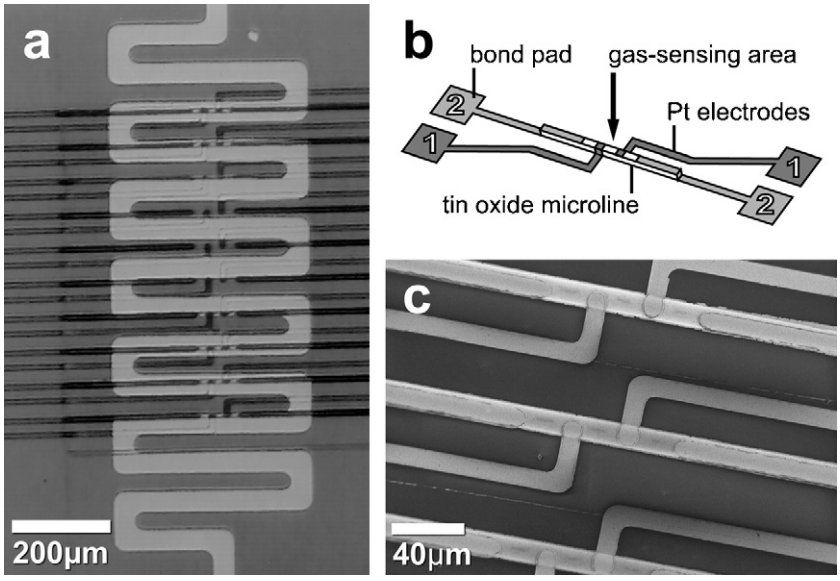

Fig. 7. (a) Top view of gas sensor set-up seen through the photoresist mask before deposition of the Pt-thin film wires for resistance measurement. Connected ceramic microlines (dark horizontal lines) and heating element were present on each substrate. (b) Schematic drawing of the contact layout for a tin oxide line. (c) SEM of micrometer thick film gas sensors. Figure reproduced from Ref. 118 with permission. Copyright Wiley-VCH Verlag GmbH & Co. KGaA.

is that the nanoparticle suspension should be well dispersed into primary particles.[143]

To increase the penetration length, Ahn et al. proposed vacuum-assisted filling of channels. Moreover, slowing down the drying process inside the channels improves the packing efficiency of suspension particles.[76,142] Some examples are shown in Fig. 8. Although lower solids contents were used than employed by Heule and Gauckler, features of the channel were replicated better because of the slower drying process. Optical waveguides[89] and micro solid oxide fuel cells[144] have been made via this approach.

An alternative solution to the problem of limited infiltration of viscous suspensions is to use a second liquid with large infiltrating capacity to help push the ceramic suspension forward and infiltrate further into the channel.[145] The second infiltrating liquid should be immiscible with the suspension, and be highly

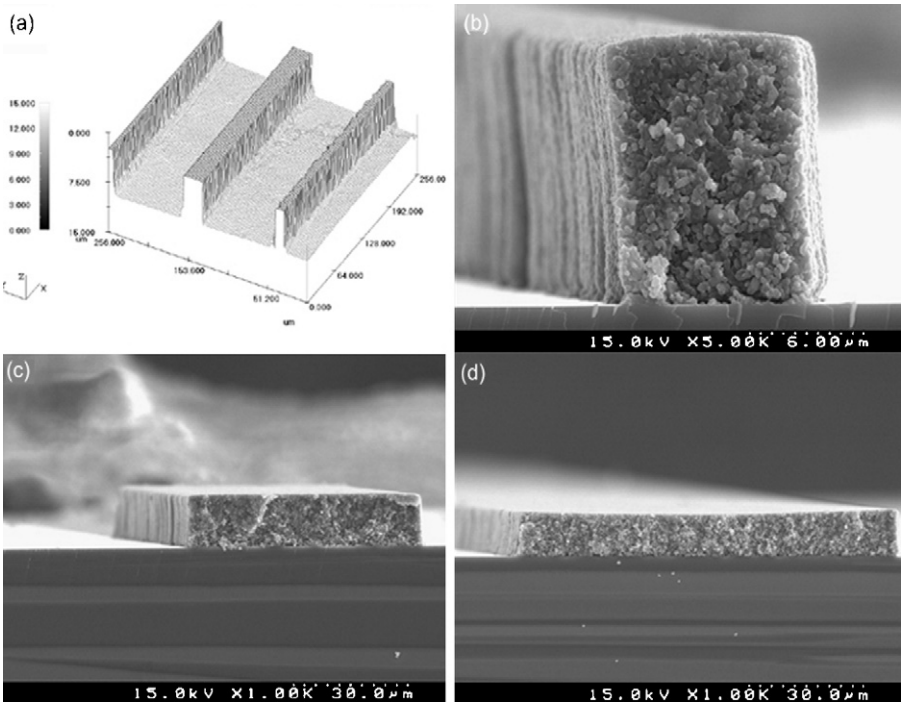

Fig. 8. (a) Three-dimensional image of thin microlines of 10–20 μm widths; (b) cross-sectional scanning electron microscopy image of a 10-μm pattern made from a dilute suspension of 5 vol% aluminum oxide. (c) Line pattern with a line width of 50 μm; (d) line with a width of 100 μm from a 20-vol% suspension. Reproduced with permission from Ref. 76. Copyright 2008 Wiley-Blackwell.

volatile, so that it can be easily removed afterwards. Under the assumption that the ceramic suspension (fluid 1 with viscosity η_1 and surface tension γ_1) has reached position z_1 inside the capillary channel at the moment ($t = 0$) that fluid 2 (with viscosity η_2 and surface tension γ_2) begins to infiltrate, the infiltration depth z_2 of fluid 2 after time t becomes[145]

$$z_2(t) = \sqrt{\frac{R(\gamma_1 - \gamma_2)t}{2\eta_2} + A^2} - A, \quad (8)$$

where $A = \eta_1 z_1/z_2$. In their experimental work, aqueous tin oxide suspensions (37 nm particles, 2 vol% solids) with a viscosity of 9 mPa s, and silicone oil were employed. An improvement of the process was reported, although the reproducibility was not optimal.

A simpler alternative to increase the rate of infiltration was proposed by Jeong, Ahn, and Moon,[89] who filled macroscopic reservoirs in direct contact with the microchannel system with a sol–gel silsesquioxane-based precursor solution. After evacuating the entire chamber to 10 Torr and then returning to atmospheric pressure, the microchannels filled within seconds.

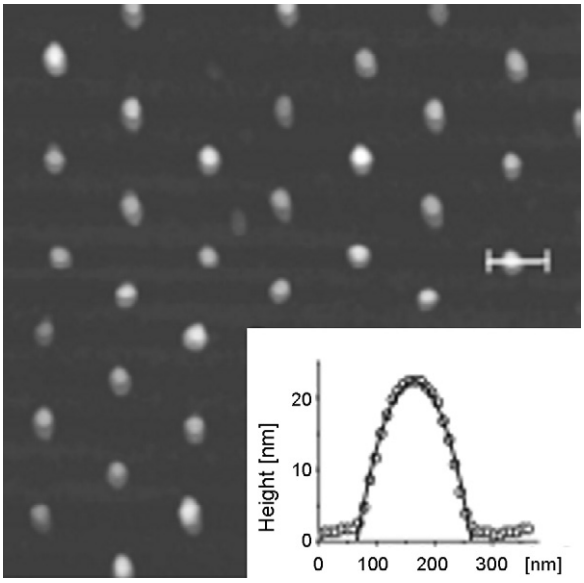

Fig. 9. AFM image (3.73 μm × 3.75 μm) of WO_3 dots. The inset shows a cross-section of the topography of a dot after annealing. The typical size (FWHM) of the dots is about 150 nm. Reprinted from Ref. 151, Copyright 2000, with permission from Elsevier.

4. Surface modification-based patterning techniques

4.1. Microcontact printing (μCP)

The first paper on microcontact printing aided metal oxide patterning was published in 1995,[146] about 2 years after the invention of microcontact printing.[7] Jeon et al. showed that by microcontact printing a hydrophobic octadecyl trichlorosilane (OTS) SAM pattern on SiO_2/Si, sapphire, indium tin oxide, or glass, the adherence of a subsequently deposited $LiNbO_3$ or $Pb_{1-3x/2}La_xTiO_3$ sol–gel film could be controlled, so that a metal oxide film formed an adhesive bond only on the non-coated areas of the surface. After pyrolysis, the amorphous layers on top of the SAM were severely cracked and showed poor adhesion. They were removed by soft mechanical polishing, and the remaining material was crystallized at 600 °C. The $LiNbO_3$ sample also showed hetero-epitaxial orientation on lattice-matched sapphire.[146]

Clem et al. made sol–gel derived Ta_2O_5 thin film capacitors with 3–4 μm lateral features and 80–120 nm thickness on Pt-coated silicon.[62] The patterns had dielectric constants of 18–25 and very low leakage currents. Payne and Clem demonstrated a multilevel example by combining selective metal–organic chemical vapour deposition (MOCVD) deposition of metal electrodes and sol–gel patterned PZT for Pt//PZT//Pt//Si(1 0 0) ferroelectric memory arrays.[147,148]

The quality of shape replication depends strongly on the site selectivity with which material is deposited on different surfaces, which in turn depends on the chemical contrast between alternate regions of the substrate.[149,150] Instead of OTS, hydrophilic 11-mercapto-undecanol (HS–$C_{11}H_{22}$–OH) SAMs have been printed on gold, while the rest of the substrate was covered with a hydrophobic octadecanethiol ($C_{18}H_{35}$–SH) SAM.[151] The thiol groups bind covalently to the gold surface, so that methyl and hydroxyl groups point outward from the surface. Features of WO_3 of 20 nm thickness formed from a WCl_6 in ethanol solution on the –OH functional hydrophilic patches. The ethanolic solution completely de-wetted from the hydrophobic areas. An AFM image of the patterned surface is shown in Fig. 9. Similarly, TiO_2 thin films were grown selectively onto OTS SAMs.[152,153] The growth rates of titania on different surfaces were found to decrease in the order –SO_3H > –NH_2 > –CH_3 > –OH. Furthermore, adhesion of oxides on methyl-terminated SAMs is poor, so that good micropatterns can be obtained when methyl-terminated SAMs are used in combination with sulfonate or amine terminal groups. An overview of the main characteristics of some commonly used SAMs for microcontact printing is shown in Table 3.[150]

Residual PDMS may also serve as patterning template. It can be realized by first treating a PDMS stamp with UV/ozone, and then making conformal contact with a substrate. A SiO_x residue will stay behind on the substrate and shield those areas

Table 3
Comparison of SAMs on silicon. Data taken from Ref. 150.

Type of SAM	Si	$Cl_3Si–C_{18}H_{37}$	$(EtO)_3Si–C_3H_6–NH_2$	Oxidized $(MeO)_3Si–C_3H_6–SH$
Functional group	–OH	–CH_3	–NH_2	–SO_3H
Water contact angle (°)	5	108	51	10
Zeta potential (mV) at pH 3	+30	0	+80	−50

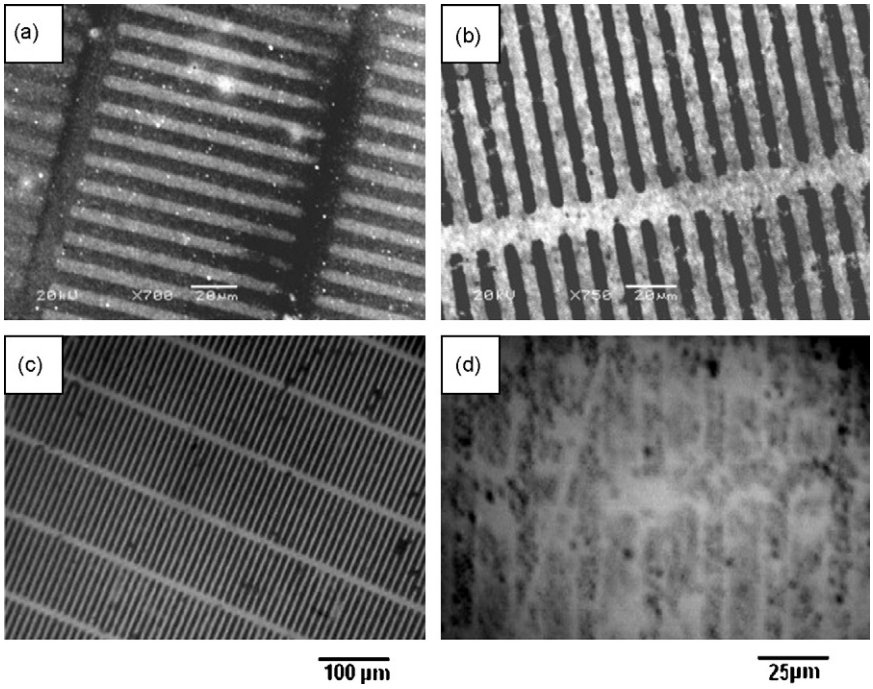

Fig. 10. (a) SEM picture of patterning SnO_2 seed layer on OTS areas by exposure to $SnCl_4$ solution for 4 h. (b) TiO_2 patterns on SnO_2 surface by immersion in peroxotitanium solution for 45 min. (c) Optical microscope images of patterned TiO_2 using SnO_2 as a seed layer; (d) optical microscope images of patterned TiO_2 without seed layer. Reprinted from Ref. 150, Copyright 2007, with permission from Elsevier.

from subsequent growth of oxide, as has been demonstrated for titania, zirconia and zinc oxide.[154,155] The resolutions are similar as with other contact printing inks.

Higher contrast than what is achievable with OTS SAMs can be accomplished by growing an oxide seed layer onto OTS prepatterned substrates by heterogeneous nucleation and growth. See Fig. 10 where titania formed primarily in areas with an SnO_2 seed layer.[150] Moreover, titania crystallized in the thermodynamically most stable rutile form, while low-temperature formation usually leads to the kinetically favoured anatase phase. At first glance it may seem surprising that tin oxide forms on OTS because the hydrophobic-hydrophilic interaction between tin oxide and OTS is unfavourable. However, the Van der Waals attraction between the two materials is probably somewhat larger. Tin oxide is also known to induce rutile phase formation.

To increase the achievable thickness of ceramic patterns, concentrated suspensions (33–45 vol%) of alumina and tin oxide particles on alkylthiol/gold and alkylsilane/silicon contrasted substrates have been used.[156] The hydrophobic–hydrophilic contrast between the SAM and the bare substrate was high, *i.e.*, 65–71° in terms of water contact angle difference. Defect-free ceramic micropatterns with a feature width of 20 μm and a thickness of 3 μm were realized after sintering at 1100 °C.

In all studies described above, the patterning step precedes the film deposition step, but the reverse sequence is also possible, as shown by Marzolin et al.[157] They deposited a wet continuous polysiloxane spin-on glass precursor, followed by microcontact printing with a reactive catalyst to convert the printed parts of the film to solid silica. A solid acid, hexadecanesulfonic acid $H_{33}C_{16}SO_3H$, gave satisfactory patterns with submicrometer resolution, and a variation in line width <100 nm. The contact time between stamp and film was found to be the key parameter that controlled the resolution that could be achieved. Short contact times resulted in poorly condensed patterns, while long contact times gave blurred patterns. This was attributed to lateral diffusion of the catalyst away from the stamp. The latter effect was observed in all experiments, as the final features of formed patterns were about 100 nm wider than the features of the stamp.

While chemically contrasted substrates have been employed widely, Jacobs and Whitesides introduced electrical microcontact printing, *i.e.*, the use of permanent electrical charge as template for the subsequent local deposition nanoparticles.[158] The concept was demonstrated by coating a patterned PDMS stamp with a thin layer of laterally conductive gold.[158,159] Then a voltage of 10–20 V was applied between the stamp and the backside of an n-type Si-supported PMMA electret substrate. The total charge that was transferred to the PMMA film was about 10–100 mC/cm^2, *i.e.*, the equivalent of 600–6000 electrons/nm^2. These charged PMMA films remained stable in air for several months. The smallest features thus obtained were about 150 nm in width. Positive charge-patterned electrets were used to form 2.5–10 μm wide lines of iron and iron oxide nanoparticles <500 nm in diameter via electrostatic interaction.

4.2. Photolithography-aided patterning

Unlike the other patterning techniques discussed in this paper, this approach is not a soft-lithographic one, since conventional photolithography instead of conformal patterning is utilized. In its simplest form, masked UV irradiation of a bare SiO_2/Si substrate leads to (exposed) areas with temporary charge

separation of electrons and holes, and (unexposed) areas without electron–hole pairs. Charged nuclei and particles, *e.g.*, titania nanoparticles made by precipitation of a $Ti(SO_4)_2$ solution with nitric acid, can be deposited preferentially onto either the exposed or the unexposed areas,[160] depending on their charge or zeta potential relative to the charge at the silicon oxide surface.

The essence of this idea was first demonstrated by Collins et al.[161] They selectively decomposed a thioacetate-terminated SAM film on a Si(1 0 0) substrate under UV light ($\lambda = 254$ nm) into a patterned sulfonate-terminated SAM:

$$=Si–C_3H_6–S–CO–CH_3 \xrightarrow{h\nu} =Si–C_3H_6–SO_3H$$

The sulfonate groups are deprotonated and negatively charged even in an acidic environment. When a 63-nm thick titania layer was grown from an acidic aqueous solution of $TiCl_4$, the formed positively charged titania moieties precipitated selectively in the $–SO_3^-$ terminated areas, yielding patterns with ~10 μm lateral resolutions.[161] The same strategy has been employed to selectively deposit zincite patterns by controlled precipitation of a zinc salt solution.[162] Initially hydrophobic SnO_2:F coated glass substrates can be patterned by masked UV irradiation ($\lambda = 185$–254 nm; fluency 14–18 mW/cm^2 for 10 min),[163] yielding a superhydrophilic surface on which anatase can be deposited by CBD. Patterned NH_3^+-functional SAMs were found to be capable of electrostatically binding negatively charged anatase nanoparticles.[164]

The strategy of using UV-patterned SAMs for site-selective deposition of functional oxides has been explored especially in a series of studies by Masuda, Koumoto, and their co-workers, and was recently reviewed.[13] In their first paper, a SiO_2/Si substrate was chemically patterned by deposition of phenyl trichlorosilane based SAM $O_{3/2}Si–C_6H_5$, followed by masked UV exposure ($\lambda \sim 185$–400 nm) to selectively cleave Si–C bonds.[165] Prior to irradiation, the SAM exhibited a contact angle of $74 \pm 2^\circ$ for water. It decreased to $<5^\circ$ after 100 min of UV exposure. Apparently, UV exposure decomposes the SAM and renders the surface hydrophilic. Anatase patterns with features of ~15 μm width were grown by a CBD process.[68,69] Material that deposited non-selectively from homogeneous nucleation and growth processes in solution was only bound to the UV-exposed hydrophilic patches, and ultrasonication was sufficient to remove any other superfluous material. The variation width of line features was generally <5%, which is sufficient for most microelectronic designs.[166] The same principle has also been demonstrated for other SAMs, such as OTS and fluorofunctional trichlorosilanes.[68,167] Alternative titanium precursors, *i.e.*, titanium dichloro diethoxide ($TiCl_2(OEt)_2$),[168] halogen-free metatitanic acid (H_2TiO_3),[169] titanium tetrachloride, and titanium tetra-ethoxide[170] gave similar results. Deposition from the gas phase using $TiCl_2(OEt)_2$ has also been demonstrated.[171] The latter films were ~20 nm thick after 2 h of deposition, which is roughly 1/6 of the growth rate in the corresponding liquid-phase processes. All these studies showed that a strong hydrophobic/hydrophilic contrast on the substrate is beneficial for generating sharp boundaries between areas where oxide deposition does and does not occur.

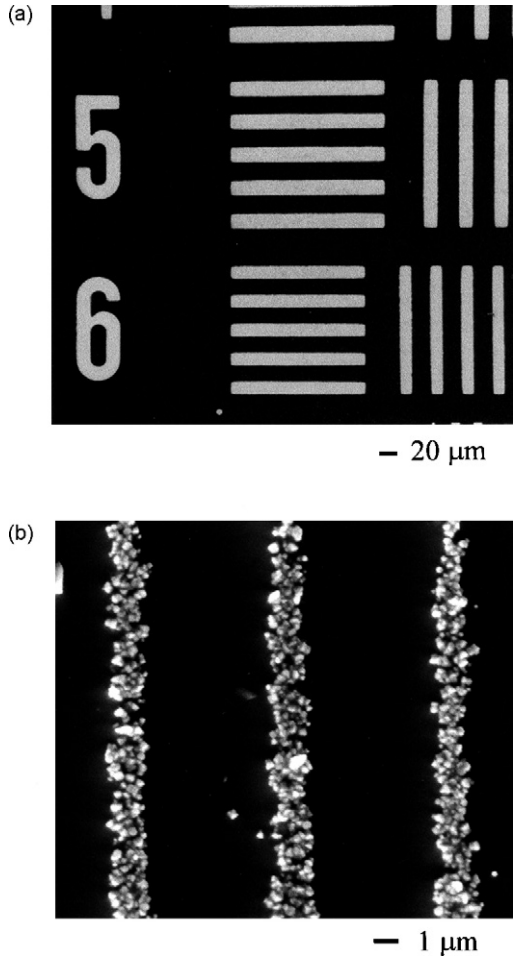

Fig. 11. SEM photographs of the as-deposited ZnO patterns. The white regions represent ZnO deposited on phenyl-terminated SAMs. (a) Overview; (b) 1 μm wide lines. The particle size is about 0.2 μm. Figure reproduced from Ref. 178 with permission. Copyright Wiley-VCH Verlag GmbH & Co. KGaA.

Many other materials were also patterned following similar CBD strategies.[56] Mixed OH/phenyl terminated surfaces were made by masked UV exposure of phenyltrichlorosilane derived SAMs, in order to make ZnF(OH),[172] SnO_2,[166] tin hydroxide,[173], La_2O_3,[174] $SrTiO_3$,[69] Ta_2O_5,[175] ZrO_2,[176] and ZnO[177–179]patterns. In the latter case Pd/Sn colloids were preadsorbed selectively on the phenyl-functionalized areas of the prepatterned substrate. These colloids catalyzed the local formation of ZnO.[179] The resulting as-deposited photoluminescent ZnO nanocrystals are shown in Fig. 11.[179,180]

When the same Pd/Sn colloids are exposed to a mixed aminosilane ($–NH_2$)/silanol (–OH)-functional patterned substrate, they adhere selectively to the amine-functional regions via electrostatic interaction. Magnetite Fe_3O_4 was deposited onto such areas.[181]

In recent years functional oxides were also micropatterned on flexible polymeric substrates, *e.g.*, polyethylene tereftalate (PET). The essential element with which a hydroxyl-terminated oxide surface can be covalently bonded to a PET surface is

3-aminopropyl triethoxysilane (APTES). This molecule can bind with its amine group to PET, and with its silane group to (surface) –OH groups. First an APTES film was formed on PET, followed by a hydrophobic organosilane-based SAM layer.[182] Then masked UV irradiation led to selective oxidation of the hydrophobic SAM so that hydrophilic patches were formed. The resulting OH-functional areas were used to selectively deposit titania.

The site selectivity with which titania is deposited can be further improved by immersing the patterned substrate in an aqueous solution of dodecylbenzene sulfonate sodium (DDBS; $C_{12}H_{25}$–C_6H_4–SO_3H) after UV exposure.[183] DDBS can adsorb on a surface in two configurations, depending on the nature of the surface. DDBS will adsorb with its –$C_{12}H_{25}$ tail oriented towards hydrophobic areas, and with its sulfonate group towards hydrophilic ones. With the shielding agent thus absorbed over the whole surface, TiO_2 was grown by aqueous CBD. During the process the hydrophobic interaction DDBS/CH_3–C_6H_4–(tolyl) remained intact. The hydrophobic patches were thereby shielded from undesired nucleation and/or deposition of titania. However, the sulfonate/OH interaction was lost quickly due to the polarity of the surrounding medium. Titania micropatterns were therefore formed on –OH-functional areas with high selectivity.

Oxygen gas has been used as a blocking medium in a study by Gao et al.[184] Gas bubbles are known to adhere selectively on hydrophobic surfaces, and can thereby block them from reaction. A lateral resolution of ~20 μm was achieved. The oxygen gas was formed as a side product in the reactions that led to formation of zirconium oxohydroxide:

$$4(ZrO)^{2+} + 8NH_4{}^{+} + 8OH^{-} + 2H_2O_2 + 8H_2O \rightarrow [Zr_4(O_2)_2(OH)_4(H_2O)_{16}]^{8+} + 8NH_3$$

$$[Zr_4(O_2)_2(OH)_4(H_2O)_{16}]^{8+} \rightarrow 4ZrO_{1.4}(OH)_{1.2} + 19.6H_2O + 2O_2(g)$$

A possibly more generally applicable approach to obtain oxide micropatterns on organic polymer substrates may be to immerse substrates into aqueous ammonium persulfate, followed by masked UV exposure. Irradiated regions of sulfate-containing biaxially oriented polypropylene (BOPP) became hydrophilic upon irradiation,[185] which is probably due to incorporation of sulfate groups into the BOPP film. Upon immersion of the polymer film in aqueous $(NH_4)_2TiF_6$/boric acid, sulfate was replaced by OH^-, onto which titania grew with high selectivity.[185] The same principle has been applied to make vertically oriented arrays of ZnO rods on BOPP.[186] When BOPP is replaced by PET, the ZnO phase deposited on the non-irradiated (hydrophobic) areas.[186] This is in accordance with other ZnO film patterning studies and has been explained by the hydrophobic nature of the ZnO crystallites.[177,187] The principle has been demonstrated for feature sizes down to 200 nm,[180] and a typical thickness of these films was 50–60 nm.[149,166] The surface roughness decreased with deposition time.

Hydrophilic seed layers increase the chemical contrast between hydrophobic and hydrophilic patches of patterned substrates, but may also enhance the nucleation and growth rate of oxides, as was demonstrated for titania and europium-doped yttrium oxide. In comparison with SAMs with silanol (–OH), amino (–NH_3^+), phenyl (–C_6H_5) and octadecyl (–$C_{18}H_{37}$) terminal groups, higher growth rates were found on amorphous titania seed layers.[149,188,189] The edge between oxide-grown patches and empty patches was sharp (<2% variation in line width), which is indicative of a high hydrophobic/hydrophilic contrast.

Several studies address the issue of spin-cast type ceramic precursors that can be directly converted into preceramic patterns by photolithography. Micrometer-scale titania and tin oxide patterns have been made by using photosensitive modified metal alkoxides.[190,191] Micropatterned ZnO nanoarrays have been made by first preparing a UV-patterned seed layer, followed by selective growth of ZnO nanorods.[192] Recently, Pham et al. developed a methacrylated polyvinylsilazane polymer photoresist that transforms into a preceramic pattern upon UV exposure.[193] The film had a Young's modulus of 4 GPa after UV curing. Subsequent pyrolysis at 800 °C converted the 10–15 μm wide features into ceramic SiCN with an elastic modulus of 45 GPa. Progress in the fabrication of SiC-based ceramic micropatterns from preceramic polymers using sacrificial templates and lithographic techniques was recently reviewed.[194]

4.3. Confocal patterning

Confocal patterning of oxides resembles microtransfer moulding, but no confinement is imposed. It is a printing rather than a moulding process, and the protruding features of the stamp are used to carry the precursor ink. Feature sizes that have been accomplished with this method are substantially larger than with the other techniques reported in this paper. The ultimate lateral resolution that can be achieved is currently >50 μm, *i.e.*, some orders of magnitude larger than what can be achieved with μTM and NIL. Control over the rheological properties of the precursor ink will be essential to control the transfer process and achieve a high resolution in the printed pattern. The concept of directly printing ceramic patterns was first demonstrated only recently[28] using a chemical solution containing a $YBa_2Cu_3O_{7-\delta}$ (YBCO) liquid precursor consisting of Cu(diethanolamine)$_2$, $Y(CF_3COO)_3$, $Ba(CF_3COO)_2$ and polyvinylpyrrolidone (PVP) in methanol. Two methods of inking the PDMS stamp were explored. In the first method a drop of the precursor was placed on a dry PDMS stamp and spun-dry. In the second approach, an "ink pad" with a wet precursor film was first made, after which the PDMS stamp was placed on the pad to pick up the precursor solution. The advantage of the first method is that thicker patterns can be made. The advantage of the second method is that no ink is present in the receded regions of the stamp, and the formation of a residual layer is avoided. In both cases the inked stamp was pressed onto the substrate and the ink was transferred. Epitaxially grown YBCO lines with (0 0 1) orientation on $LaAlO_3$(0 0 1) single-crystalline substrates were generated in this manner. The lines became superconductive below 85 K.

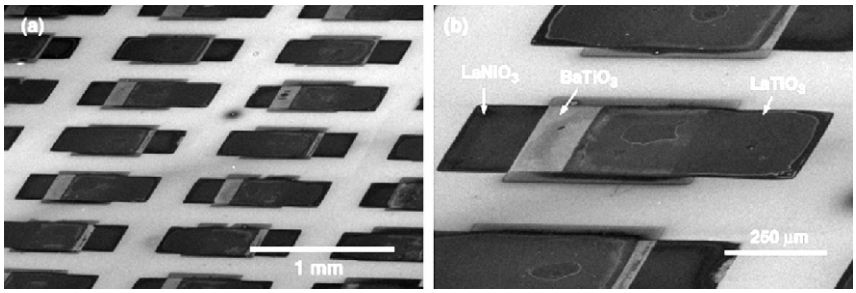

Fig. 12. Scanning electron microscopy images of (a) an array of microcontact-printed single-layer thin film capacitors of $LaNiO_3/BaTiO_3/LaNiO_3$; (b) close-up of one capacitor. Reproduced with permission from Ref. 195. Copyright 2006 Wiley-Blackwell.

The same patterning methods were also applied to make Cu features from $Cu(diethanolamine)_2$.

Nagata used confocal printing to pattern dielectric $BaTiO_3$ and conducting $LaNiO_3$ thin films for multilayer capacitors.[195] The PDMS stamp was pretreated in oxygen plasma as discussed in Section 2.2. Single-layer $BaTiO_3$ patterned capacitors of <200 nm thickness on Ni foil with a dielectric constant >800 and loss tangent <2% were printed. An example is shown in Fig. 12. Stacked $BaTiO_3/LaNiO_3$ multilayers with layer thicknesses of 200 and 30 nm, respectively, were also demonstrated.

Similarly, iron oxide and nickel-containing nanoparticles have been printed on silicon[196] from ethanolic $NiCl_2$ and $FeCl_3$ solutions. After inking the stamp was dried to evaporate ethanol and oxidize the metal chlorides to Fe_2O_3 and Ni-containing nanoparticles. The particles on the protruding areas of the stamp were transferred to the substrate via conformal contact, and served as catalysts for the subsequent local growth of carbon nanotubes[196] and the conductive polymer poly(3,4-ethylenedioxythiophene) (PEDOT).[197]

5. Conclusions

Many kinds of ceramic materials and hybrids have been patterned in recent years on micrometer and submicrometer-scale, and nanoscale objects with feature sizes smaller than 100 nm have been reported in literature. Especially with micromoulding, a technique very similar to nanoimprint lithography, very small features can be made with high fidelity. Nonetheless, the fabrication of truly high-aspect ratio structures still remains a challenge. Well-defined submicrometer-scale objects with aspect ratios >1 are rarely reported. Furthermore, a fundamental problem concerns the low solids content in precursor solutions and ceramic suspensions. While solids content up to ~40 vol% may be possible in suspensions, much lower solids concentrations (typically <10 vol%) are present in solution-based precursors such as sol–gels. The shrinkage after a pattern has been defined and a wet film has been deposited is therefore considerable. This makes precise shape replication of a mould very difficult, if not impossible.

Besides improvement of lateral resolution and the possibility to register patterns in order to allow multiple layer fabrication,[12] a very important development concerns the ability to pattern ceramics on polymeric substrates. The ability to do so will open up many new possibilities to incorporate functional ceramic materials into low-cost polymer-based devices. A few studies with promising results have already been published in recent years on this topic.[182,185]

Acknowledgements

Financial support from the Netherlands Technology Foundation STW within the framework of the VIDI Innovational Research Scheme is acknowledged.

References

1. Xia YN, Rogers JA, Paul KE, Whitesides GM. Unconventional methods for fabricating and patterning nanostructures. *Chem Rev* 1999;**99**:1823–48.
2. Geissler M, Xia YN. Patterning: principles and some new developments. *Adv Mater* 2004;**16**:1249–69.
3. Gates BD, Xu QB, Stewart M, Ryan D, Willson CG, Whitesides GM. New approaches to nanofabrication: molding, printing, and other techniques. *Chem Rev* 2005;**105**:1171–96.
4. Henzie J, Barton JE, Stender CL, Odom TW. Large-area nanoscale patterning: chemistry meets fabrication. *Acc Chem Res* 2006;**39**:249–57.
5. del Campo A, Arzt E. Fabrication approaches for generating complex micro- and nanopatterns on polymeric surfaces. *Chem Rev* 2008;**108**:911–45.
6. Heule M, Vuillemin S, Gauckler LJ. Powder-based ceramic meso- and microscale fabrication processes. *Adv Mater* 2003;**15**:1237–45.
7. Kumar A, Whitesides GM. Features of gold having micrometer to centimeter dimensions can be formed through a combination of stamping with an elastomeric stamp and an alkanethiol ink followed by chemical ething. *Appl Phys Lett* 1993;**63**:2002–4.
8. Zhao XM, Xia YN, Whitesides GM. Fabrication of three-dimensional micro-structures: microtransfer molding. *Adv Mater* 1996;**8**:837–40.
9. Xia YN, Whitesides GM. Soft lithography. *Annu Rev Mater Sci* 1998;**28**:153–84.
10. Martin CR, Aksay IA. Submicrometer-scale patterning of ceramic thin films. *J Electroceram* 2004;**12**:53–68.
11. Rogers JA, Nuzzo RG. Recent progress in soft lithography. *Mater Today* 2005;**8**:50–6.
12. Folch A, Schmidt MA. Wafer-level in-registry microstamping. *J Microelectromech Syst* 1999;**8**:85–9.
13. Masuda Y. Liquid phase patterning of ceramics. *J Ceram Soc Jpn* 2007;**115**:101–9.
14. Koumoto K, Saito N, Gao YF, Masuda Y, Zhu PX. Nano/micro patterning of inorganic thin films. *Bull Chem Soc Jpn* 2008;**81**:1337–76.
15. Huang WH, Li J, Luo CX, Zhang JL, Luan SF, Han YC. Different colloids self-assembly in micromolding. *Colloid Surf A: Physicochem Eng Aspects* 2006;**273**:43–6.
16. Huang WH, Li JA, Xue LJ, Xing RB, Luan SF, Luo CX, et al. Complex aggregates of spherical colloids via modified micromolding in capillaries. *Colloid Surf A: Physicochem Eng Aspects* 2006;**278**:144–8.

17. Yamauchi Y, Imasu J, Kuroda Y, Kuroda K, Sakka Y. Facile patterning of assembled silica nanoparticles with a closely packed arrangement through guided growth. *J Mater Chem* 2009;**19**:1964–7.
18. Lee DH, Chang YJ, Herman GS, Chang CH. A general route to printable high-mobility transparent amorphous oxide semiconductors. *Adv Mater* 2007;**19**:843–7.
19. Su M, Liu XG, Li SY, Dravid VP, Mirkin CA. Moving beyond molecules: patterning solid-state features via dip-pen nanolithography with sol-based inks. *J Am Chem Soc* 2002;**124**:1560–1.
20. Fu L, Liu XG, Zhang Y, Dravid VP, Mirkin CA. Nanopatterning of "hard" magnetic nanostructures via dip-pen nanolithography and a sol-based ink. *Nano Lett* 2003;**3**:757–60.
21. Salaita K, Wang YH, Mirkin CA. Applications of dip-pen nanolithography. *Nat Nanotechnol* 2007;**2**:145–55.
22. Lewis JA. Direct ink writing of 3D functional materials. *Adv Funct Mater* 2006;**16**:2193–204.
23. Lee JN, Park C, Whitesides GM. Solvent compatibility of poly(dimethylsiloxane)-based microfluidic devices. *Anal Chem* 2003;**75**: 6544–54.
24. Chou SY, Krauss PR, Renstrom PJ. Imprint lithography with 25-nanometer resolution. *Science* 1996;**272**:85–7.
25. Chou SY, Krauss PR, Renstrom PJ. Nanoimprint lithography. *J Vac Sci Technol B* 1996;**14**:4129–33.
26. Guo LJ. Nanoimprint lithography: methods and material requirements. *Adv Mater* 2007;**19**:495–513.
27. Kim E, Xia YN, Whitesides GM. Micromolding in capillaries: applications in materials science. *J Am Chem Soc* 1996;**118**:5722–31.
28. Chang NA, Richardson JJ, Clem PG, Hsu JWP. Additive patterning of conductors and superconductors by solution stamping nanolithography. *Small* 2006;**2**:75–9.
29. Bietsch A, Michel B. Conformal contact and pattern stability of stamps used for soft lithography. *J Appl Phys* 2000;**88**:4310–8.
30. Sharp KG, Blackman GS, Glassmaker NJ, Jagota A, Hui CY. Effect of stamp deformation on the quality of microcontact printing: theory and experiment. *Langmuir* 2004;**20**:6430–8.
31. Huang YGY, Zhou WX, Hsia KJ, Menard E, Park JU, Rogers JA, et al. Stamp collapse in soft lithography. *Langmuir* 2005;**21**:8058–68.
32. Roca-Cusachs P, Rico F, Martinez E, Toset J, Farre R, Navajas D. Stability of microfabricated high aspect ratio structures in poly(dimethylsiloxane). *Langmuir* 2005;**21**:5542–8.
33. Lee TW, Mitrofanov O, Hsu JWR. Pattern-transfer fidelity in soft lithography: the role of pattern density and aspect ratio. *Adv Funct Mater* 2005;**15**:1683–8.
34. Odom TW, Love JC, Wolfe DB, Paul KE, Whitesides GM. Improved pattern transfer in soft lithography using composite stamps. *Langmuir* 2002;**18**:5314–20.
35. Schmid H, Michel B. Siloxane polymers for high-resolution, high-accuracy soft lithography. *Macromolecules* 2000;**33**:3042–9.
36. Choi KM, Rogers JA. A photocurable poly(dimethylsiloxane) chemistry designed for soft lithographic molding and printing in the nanometer regime. *J Am Chem Soc* 2003;**125**:4060–1.
37. Viallet B, Gallo P, Daran E. Nanoimprint process using epoxy-slioxane low-viscosity prepolymer. *J Vac Sci Technol B* 2005;**23**:72–5.
38. Kim WS, Choi DG, Bae BS. Ultraviolet-nanoimprint of 40 nm scale patterns using functionally modified fluorinated hybrid materials. *Nanotechnology* 2006;**17**:3319–24.
39. Gratton SEA, Williams SS, Napier ME, Pohlhaus PD, Zhou ZL, Wiles KB, et al. The pursuit of a scalable nanofabrication platform for use in material and life science applications. *Acc Chem Res* 2008;**41**:1685–95.
40. Truong TT, Lin RS, Jeon S, Lee HH, Maria J, Gaur A, et al. Soft lithography using acryloxy perfluoropolyether composite stamps. *Langmuir* 2007;**23**:2898–905.
41. Pina-Hernandez C, Fu PF, Guo LJ. Easy duplication of stamps using UV cured fluoro-silsesquioxane for nanoimprint lithography. *J Vac Sci Technol B* 2008;**26**:2426–9.
42. Kim JY, Choi DG, Jeong JH, Lee ES. UV-curable nanoimprint resin with enhanced anti-sticking property. *Appl Surf Sci* 2008;**254**:4793–6.
43. Langowski BA, Uhrich KE. Oxygen plasma-treatment effects on Si transfer. *Langmuir* 2005;**21**:6366–72.
44. Glasmastar K, Gold J, Andersson AS, Sutherland DS, Kasemo B. Silicone transfer during microcontact printing. *Langmuir* 2003;**19**:5475–83.
45. Hale PS, Kappen P, Prissanaroon W, Brack N, Pigram PJ, Liesegang J. Minimizing silicone transfer during micro-contact printing. *Appl Surf Sci* 2007;**253**:3746–50.
46. Wigenius JA, Hamedi M, Inganas O. Limits to nanopatterning of fluids on surfaces in soft lithography. *Adv Funct Mater* 2008;**18**:2563–71.
47. Graham DJ, Price DD, Ratner BD. Solution assembled and microcontact printed monolayers of dodecanethiol on gold: a multivariate exploration of chemistry and contamination. *Langmuir* 2002;**18**:1518–27.
48. Roman GT, Culbertson CT. Surface engineering of poly(dimethylsiloxane) microfluidic devices using transition metal sol–gel chemistry. *Langmuir* 2006;**22**:4445–51.
49. Pisignano D, Di Benedetto F, Persano L, Gigli G, Cingolani R. Rapid soft lithography by bottom-up enhanced capillarity. *Langmuir* 2004;**20**:4802–4.
50. Wang B, Oleschuk RD, Horton JH. Chemical force titrations of amine- and sulfonic acid-modified poly(dimethylsiloxane). *Langmuir* 2005;**21**:1290–8.
51. He QG, Liu ZC, Xiao PF, Liang RQ, He NY, Lu ZH. Preparation of hydrophilic poly(dimethylsiloxane) stamps by plasma-induced grafting. *Langmuir* 2003;**19**:6982–6.
52. Barbier V, Tatoulian M, Li H, Arefi-Khonsari F, Ajdari A, Tabeling P. Stable modification of PDMS surface properties by plasma polymerization: application to the formation of double emulsions in microfluidic systems. *Langmuir* 2006;**22**:5230–2.
53. Lee J, Kim MJ, Lee HH. Surface modification of poly(dimethylsiloxane) for retarding swelling in organic solvents. *Langmuir* 2006;**22**:2090–5.
54. Schwartz RW. Chemical solution deposition of perovskite thin films. *Chem Mater* 1997;**9**:2325–40.
55. Schwartz RW, Schneller T, Waser R. Chemical solution deposition of electronic oxide films. *C R Chim* 2004;**7**:433–61.
56. Parikh H, De Guire MR. Recent progress in the synthesis of oxide films from liquid solutions. *J Ceram Soc Jpn* 2009;**117**:228–35.
57. Wright JD, Sommerdijk NAJM. *Sol–gel materials. Chemistry and applications*. Boca Raton, FL: CRC Press; 2001.
58. Tohge N, Matsuda A, Minami T, Matsuno Y, Katayama S, Ikeda Y. Fine-patterning on glass substrates by the sol–gel method. *J Non-Cryst Solids* 1988;**100**:501–5.
59. Krug H, Merl N, Schmidt H. Fine patterning of thin sol–gel films. *J Non-Cryst Solids* 1992;**147–148**:447–50.
60. Marzolin C, Smith SP, Prentiss M, Whitesides GM. Fabrication of glass microstructures by micro-molding of sol–gel precursors. *Adv Mater* 1998;**10**:571–4.
61. Kim WS, Yoon KB, Bae BS. Nanopatterning of photonic crystals with a photocurable silica-titania organic–inorganic hybrid material by a UV-based nanoimprint technique. *J Mater Chem* 2005;**15**:4535–9.
62. Clem PG, Jeon NL, Nuzzo RG, Payne DA. Monolayer-mediated deposition of tantalum(V) oxide thin film structures from solution precursors. *J Am Ceram Soc* 1997;**80**:2821–7.
63. Hampton MJ, Williams SS, Zhou Z, Nunes J, Ko DH, Templeton JL, et al. The patterning of sub-500 nm inorganic oxide structures. *Adv Mater* 2008;**20**:2667–73.
64. Goh C, Coakley KM, McGehee MD. Nanostructuring titania by embossing with polymer molds made from anodic alumina templates. *Nano Lett* 2005;**5**:1545–9.
65. Martin CR, Aksay IA. Topographical evolution of lead zirconate titanate (PZT) thin films patterned by micromolding in capillaries. *J Phys Chem B* 2003;**107**:4261–8.
66. Kim JH, Lange FF, Cheon CI. Epitaxial growth of patterned $SrBi_2Ta_2O_9$ lines by channel stamping. *J Mater Res* 1999;**14**:1194–6.
67. Harnagea C, Alexe M, Schilling J, Choi J, Wehrspohn RB, Hesse D, et al. Mesoscopic ferroelectric cell arrays prepared by imprint lithography. *Appl Phys Lett* 2003;**83**:1827–9.

68. Masuda Y, Sugiyama T, Koumoto K. Micropatterning of anatase TiO_2 thin films from an aqueous solution by a site-selective immersion method. *J Mater Chem* 2002;**12**:2643–7.
69. Gao YF, Masuda Y, Yonezawa T, Koumoto K. Site-selective deposition and micropatterning of $SrTiO_3$ thin film on self-assembled monolayers by the liquid phase deposition method. *Chem Mater* 2002;**14**:5006–14.
70. Göbel OF, Nedelcu M, Steiner U. Soft lithography of ceramic patterns. *Adv Funct Mater* 2007;**17**:1131–6.
71. Zou G, You X, He PS. Patterning of nanocrystalline $La_{0.7}Sr_{0.3}MnO_3$ thin films prepared by sol–gel process combined with soft lithography. *Mater Lett* 2008;**62**:1785–8.
72. Schneider A, Su B, Button TW, Singleton L, Wilhelmi O, Huq SE, et al. Comparison of PMMA and SU-8 resist moulds for embossing of PZT to produce high-aspect-ratio microstructures using LIGA process. *Microsyst Technol* 2002;**8**:88–92.
73. Heule M, Schell J, Gauckler LJ. Powder-based tin oxide microcomponents on silicon substrates fabricated by micromolding in capillaries. *J Am Ceram Soc* 2003;**86**:407–12.
74. Pisignano D, Sariconi E, Mazzeo M, Gigli G, Cingolani R. High-temperature microfluidic lithography. *Adv Mater* 2002;**14**:1565–7.
75. Moran PM, Lange FF. Microscale lithography via channel stamping: relationships between capillarity, channel filling, and debonding. *Appl Phys Lett* 1999;**74**:1332–4.
76. Ahn S-J, Min JH, Kim J, Moon J. Process mechanism for vacuum-assisted microfluidic lithography with ceramic colloidal suspensions. *J Am Ceram Soc* 2008;**91**:2143–9.
77. Seemann R, Kramer EJ, Lange FF. Patterning of polymers: precise channel stamping by optimizing wetting properties. *New J Phys* 2004;**6**:111.
78. Seemann R, Brinkmann M, Kramer EJ, Lange FF, Lipowsky R. Wetting morphologies at microstructured surfaces. *Proc Natl Acad Sci USA* 2005;**102**:1848–52.
79. Matsuda A, Sasaki T, Tatsumisago M, Minami T. Micropatterning on methylsilsesquioxane-phenylsilsesquioxane thick films by the sol–gel method. *J Am Ceram Soc* 2000;**83**:3211–3.
80. Khan SU, Göbel OF, Blank DHA, ten Elshof JE. Patterning lead zirconate titanate nanostructures at sub-200 nm resolution by soft confocal imprint lithography and nano-transfer molding. *ACS Appl Mater Interfaces* 2009;**1**:2250–5.
81. Yang PD, Wirnsberger G, Huang HC, Cordero SR, McGehee MD, Scott B, et al. Mirrorless lasing from mesostructured waveguides patterned by soft lithography. *Science* 2000;**287**:465–7.
82. Su B, Zhang D, Button TW. Micropatterning of fine scale ceramic structures. *J Mater Sci* 2002;**37**:3123–6.
83. Zhang D, Su B, Button TW. Preparation of concentrated aqueous alumina suspensions for soft-molding microfabrication. *J Eur Ceram Soc* 2004;**27**:231–7.
84. Zhang D, Su B, Button TW. Improvements in the structural integrity of green ceramic microcomponents by a modified soft moulding process. *J Eur Ceram Soc* 2007;**27**:645–50.
85. Schönholzer UP, Gauckler LJ. Ceramic parts patterned in the micrometer range. *Adv Mater* 1999;**11**:630–2.
86. Bulthaup CA, Wilhelm EJ, Hubert BN, Ridley BA, Jacobson JM. All-additive fabrication of inorganic logic elements by liquid embossing. *Appl Phys Lett* 2001;**79**:1525–7.
87. Göbel OF, Blank DHA, ten Elshof JE. Thin films of conductive ZnO patterned by micromolding resulting in nearly isolated features. *ACS Appl Mater Interfaces* 2010, doi:10.1021/am9007374.
88. Matsuda A, Matsuno Y, Tatsumisago M, Minami T. Fine patterning and characterization of gel firms derived from methyltriethoxysilane and tetraethoxysilane. *J Am Ceram Soc* 1998;**81**:2849–52.
89. Jeong S, Ahn S-J, Moon J. Fabrication of patterned inorganic–organic hybrid film for the optical waveguide by microfluidic lithography. *J Am Ceram Soc* 2005;**88**:1033–6.
90. Schueller OJA, Whitesides GM, Rogers JA, Meier M, Dodabalapur A. Fabrication of photonic crystal lasers by nanomolding of solgel glasses. *Appl Opt* 1999;**38**:5799–802.
91. Ro HW, Jones RL, Peng H, Hines DR, Lee HJ, Lin EK, et al. The direct patterning of nanoporous interlayer dielectric insulator films by nanoimprint lithography. *Adv Mater* 2007;**19**:2919–24.
92. Yang PD, Deng T, Zhao DY, Feng PY, Pine D, Chmelka BF, et al. Hierarchically ordered oxides. *Science* 1998;**282**:2244–6.
93. Ro HW, Peng H, Niihara KI, Lee HJ, Lin EK, Karim A, et al. Self-sealing of nanoporous low dielectric constant patterns fabricated by nanoimprint lithography. *Adv Mater* 2008;**20**:1934–9.
94. Verschuuren M, Van Sprang H. D photonic structures by sol–gel imprint lithography. In: Gingli G, editor. *Materials research society symposium proceedings, vol. 1002E*. Warrendale, PA: Materials Research Society; 2007. N03-05.
95. Kim WS, Lee JH, Shin SY, Bae BS, Kim YC. Fabrication of ridge waveguides by UV embossing and stamping of sol–gel hybrid materials. *IEEE Photon Technol Lett* 2004;**16**:1888–90.
96. Choi DG, Jeong JH, Sim YS, Lee ES, Kim WS, Bae BS. Fluorinated organic–inorganic hybrid mold as a new stamp for nanoimprint and soft lithography. *Langmuir* 2005;**21**:9390–2.
97. Kim WS, Kim KS, Kim YC, Bae BS. Thermowetting embossing nanoimprinting of the organic–inorganic hybrid materials. *Thin Solid Films* 2005;**476**:181–4.
98. Kim WS, Jin JH, Bae BS. Low adhesive force of fluorinated sol–gel hybrid materials for easy de-moulding in a UV-based nano-imprint process. *Nanotechnology* 2006;**17**:1212–6.
99. Kim WS, Kim KS, Eo YJ, Yoon Y, Bae BS. Synthesis of fluorinated hybrid material for UV embossing of a large core optical waveguide structure. *J Mater Chem* 2005;**15**:465–9.
100. Alexe M, Harnagea C, Hesse D. Non-conventional micro- and nanopatterning techniques for electroceramics. *J Electroceram* 2004;**12**:69–88.
101. Hsieh KC, Chen HL, Lin CH, Lee CY. Directly patterning ferroelectric films by nanoimprint innography with low temperature and low pressure. *J Vac Sci Technol B* 2006;**24**:3234–8.
102. Chen HL, Hsieh KC, Lin CH, Chen SH. Using direct nanoimprinting of ferroelectric films to prepare devices exhibiting bi-directionally tunable surface plasmon resonances. *Nanotechnology* 2008;**19**:435304.
103. Shi G, Lu N, Gao L, Xu H, Yang B, Li Y, et al. Fabrication of TiO_2 arrays using solvent-assisted soft lithography. *Langmuir* 2009;**25**:9639–43.
104. George A, Blank DHA, ten Elshof JE. Nanopatterning from the gas phase: high resolution soft lithographic patterning of organosilane thin films. *Langmuir* 2009;**25**:13298–301.
105. Schönholzer UP, Stutzmann N, Tervoort TA, Smith P, Gauckler LJ. Micropatterned ceramics by casting into polymer molds. *J Am Ceram Soc* 2002;**85**:1885–7.
106. Yi DK, Yoo SJ, Kim DY. Spin-on-based fabrication of titania nanowires using a sol–gel process. *Nano Lett* 2002;**2**:1101–4.
107. Martin CR, Aksay IA. Microchannel molding: a soft lithography-inspired approach to micrometer-scale patterning. *J Mater Res* 2005;**20**:1995–2003.
108. Auger MA, Schilardi PL, Caretti I, Sanchez O, Benitez G, Albella JM, et al. Molding and replication of ceramic surfaces with nanoscale resolution. *Small* 2005;**1**:300–9.
109. Deki S, Iizuka S, Horie A, Mizuhata M, Kajinami A. Liquid-phase infiltration (LPI) process for the fabrication of highly nano-ordered materials. *Chem Mater* 2004;**16**:1747–50.
110. Deki S, Iizuka S, Horie A, Mizuhata M, Kajinami A. Nanofabrication of metal oxide thin films and nano-ceramics from aqueous solution. *J Mater Chem* 2004;**14**:3127–32.
111. Kim SS, Chun C, Hong JC, Kim DY. Well-ordered TiO_2 nanostructures fabricated using surface relief gratings on polymer films. *J Mater Chem* 2006;**16**:370–5.
112. Dravid VP. "Controlling" internal microstructure of nanopatterned oxides via soft electron beam lithography (soft-eBL). *J Mater Chem* 2009;**19**:4295–9.
113. Donthu S, Pan ZX, Myers B, Shekhawat G, Wu NG, Dravid V. Facile scheme for fabricating solid-state nanostructures using e-beam lithography and solution precursors. *Nano Lett* 2005;**5**:1710–5.

114. Donthu S, Sun T, Dravid V. Fabrication and structural evaluation of beaded inorganic nanostructures using soft electron-beam lithography. *Adv Mater* 2007;**19**:125–8.
115. Pan ZX, Donthu SK, Wu NQ, Li SY, Dravid VP. Directed fabrication of radially stacked multifunctional oxide heterostructures using soft electron-beam lithography. *Small* 2006;**2**:274–80.
116. Sun T, Pan ZX, Dravid VP, Wang ZY, Yu MF, Wang J. Nanopatterning of multiferroic $BiFeO_3$ using "soft" electron beam lithography. *Appl Phys Lett* 2006;**89**:3.
117. Pan Z, Li S, Wang Z, Yu MF, Dravid VP. Patterning-controlled morphology of spatially and dimensionally constrained oxide nanostructures. *Appl Phys Lett* 2007;**91**:3.
118. Heule M, Gauckler LJ. Gas sensors fabricated from ceramic suspensions by micromolding in capillaries. *Adv Mater* 2001;**13**:1790–3.
119. Jeon NL, Hu JM, Whitesides GM, Erhardt MK, Nuzzo RG. Fabrication of silicon MOSFETs using soft lithography. *Adv Mater* 1998;**10**:1466–9.
120. Kim E, Whitesides GM. Imbibition and flow of wetting liquids in noncircular capillaries. *J Phys Chem B* 1997;**101**:855–63.
121. Huang WF, Liu QS, Li Y. Capillary filling flows inside patterned-surface microchannels. *Chem Eng Technol* 2006;**29**:716–23.
122. Kim DS, Lee KC, Kwon TH, Lee SS. Micro-channel filling flow considering surface tension effect. *J Micromech Microeng* 2002;**12**:236–46.
123. Jeon NL, Choi IS, Xu B, Whitesides GM. Large-area patterning by vacuum-assisted micromolding. *Adv Mater* 1999;**11**:946–50.
124. Beh WS, Xia Y, Qin D. Formation of patterned microstructures of polycrystalline ceramics from precursor polymers using micromolding in capillaries. *J Mater Res* 1999;**14**:3995–4003.
125. Vartuli JS, Ozenbas M, Chun CM, Trau M, Aksay IA. Micropatterned lead zirconium titanate thin films. *J Mater Res* 2003;**18**:1259–65.
126. Seraji S, Wu Y, Jewell-Larson NE, Forbess MJ, Limmer SJ, Chou TP, et al. Patterned microstructure of sol–gel derived complex oxides using soft lithography. *Adv Mater* 2000;**12**:1421–4.
127. Cheng ZY, Wang Z, Xing RB, Han YC, Lin J. Patterning and photoluminescent properties of perovskite-type organic/inorganic hybrid luminescent films by soft lithography. *Chem Phys Lett* 2003;**376**:481–6.
128. Yu M, Lin J, Wang Z, Fu J, Wang S, Zhang HJ, et al. Fabrication, patterning, and optical properties of nanocrystalline YVO_4:A (A = Eu^{3+}, Dy^{3+}, Sm^{3+}, Er^{3+}) phosphor films via sol–gel soft lithography. *Chem Mater* 2002;**14**:2224–31.
129. Han XM, Lin J, Xing RB, Fu J, Wang SB, Han YC. Preparation, patterning and luminescent properties of oxyapatite $La_{9.33}(SiO_6)(4)O_2$:A (A = Eu^{3+}, Tb^{3+}, Ce^{3+}) phosphor films by sol–gel soft lithography. *J Phys Condens Matter* 2003;**15**:2115–26.
130. Pang ML, Lin J, Cheng ZY, Fu J, Xing RB, Wang SB. Patterning and luminescent properties of nanocrystallineY_2O_3:Eu^{3+} phosphor films by sol–gel soft lithography. *Mater Sci Eng B: Solid State Mater Adv Technol* 2003;**100**:124–31.
131. Han XM, Lin J, Fu J, Xing RB, Yu M, Zhou YH, et al. Fabrication, patterning and luminescence properties of X_2–Y_2SiO_5:A (A = Eu^{3+}, Tb^{3+}, Ce^{3+}) phosphor films via sol–gel soft lithography. *Solid State Sci* 2004;**6**:349–55.
132. Han XM, Lin J, Xing RB, Fu J, Wang SB. Patterning and optical properties Rhodamine B-doped organic–inorganic silica films fabricated by sol–gel soft lithography. *Mater Lett* 2003;**57**:1355–60.
133. Park KH, Sung IK, Kim DP. A facile route to prepare high surface area mesoporous SiC from SiO_2 sphere templates. *J Mater Chem* 2004;**14**:3436–9.
134. Lee DH, Park KH, Hong LY, Kim DP. SiCN ceramic patterns fabricated by soft lithography techniques. *Sens Actuat A: Phys* 2007;**135**:895–901.
135. Trau M, Yao N, Kim E, Xia Y, Whitesides GM, Aksay IA. Microscopic patterning of orientated mesoscopic silica through guided growth. *Nature* 1997;**390**:674–6.
136. Wirnsberger G, Yang PD, Huang HC, Scott B, Deng T, Whitesides GM, et al. Patterned block-copolymer-silica mesostructures as host media for the laser dye rhodamine 6G. *J Phys Chem B* 2001;**105**:6307–13.
137. Yang PD, Rizvi AH, Messer B, Chmelka BF, Whitesides GM, Stucky GD. Patterning porous oxides within microchannel networks. *Adv Mater* 2001;**13**:427–31.
138. Kim WS, Kim MG, Ahn JH, Bae BS, Park CB. Protein micropatterning on bifunctional organic–inorganic sol–gel hybrid materials. *Langmuir* 2007;**23**:4732–6.
139. de la Rica R, Baldi A, Mendoza E, Paulo AS, Llobera A, Fernandez-Sanchez C. Silane nanopatterns via gas-phase soft lithography. *Small* 2008;**4**:1076–9.
140. Heule M, Gauckler LJ. Micromachined nanoparticulate ceramic gas sensor array on MEMS substrates. In: *Materials research society symposium proceedings, vol. 687*. 2002. p. B4.5.1–6.
141. Heule M, Gauckler LJ. Miniaturised arrays of tin oxide gas sensors on single microhotplate substrates fabricated by micromolding in capillaries. *Sens Actuat B* 2003;**93**:100–6.
142. Ahn S-J, Moon J. Vacuum-assisted microfluidic lithography of ceramic microstructures. *J Am Ceram Soc* 2005;**88**:1171–4.
143. Imasu J, Sakka Y. Large-scale patterning of TiO_2 nano powders using micro molds. *J Ceram Soc Jpn* 2007;**115**:697–700.
144. Ahn S-J, Lee JH, Kim J, Moon J. Single-chamber solid oxide fuel cell with micropatterned interdigitated electrodes. *Electrochem Solid State Lett* 2006;**9**:A228–31.
145. Imasu J, Fudouzi H, Sakka Y. Micro-scale patterning of ceramic colloidal suspension by micro molding in capillaries (MIMIC) with assistance of highly infiltrating liquid. *J Ceram Soc Jpn* 2006;**114**:725–8.
146. Jeon NL, Clem PG, Nuzzo RG, Payne DA. Patterning of dielectric oxide thin-layers by microcontact printing of self-assembled monolayers. *J Mater Res* 1995;**10**:2996–9.
147. Jeon NL, Clem P, Jung DY, Lin WB, Girolami GS, Payne DA, et al. Additive fabrication of integrated ferroelectric thin-film capacitors using self-assembled organic thin-film templates. *Adv Mater* 1997;**9**:891–5.
148. Payne DA, Clem PG. Monolayer-mediated patterning of integrated electroceramics. *J Electroceram* 1999;**3**:163–72.
149. Masuda Y, Ieda S, Koumoto K. Site-selective deposition of anatase TiO_2 in an aqueous solution using a seed layer. *Langmuir* 2003;**19**:4415–9.
150. Liang S, Chen M, Xue QJ, Qi YL, Chen JM. Site selective micro-patterned rutile TiO_2 film through a seed layer deposition. *J Colloid Interface Sci* 2007;**311**:194–202.
151. Bechinger C, Muffler H, Schafle C, Sundberg O, Leiderer P. Submicron metal oxide structures by a sol–gel process on patterned substrates. *Thin Solid Films* 2000;**366**:135–8.
152. Liang S, Chen M, Xue QJ. Deposition behaviors and patterning of TiO_2 thin films on different SAMS surfaces from titanium sulfate aqueous solution. *Colloid Surf A: Physicochem Eng Aspects* 2008;**324**:137–42.
153. Park MH, Jang YJ, Sung-Suh HM, Sung MM. Selective atomic layer deposition of titanium oxide on patterned self-assembled monolayers formed by microcontact printing. *Langmuir* 2004;**20**:2257–60.
154. Park KS, Seo EK, Do YR, Kim K, Sung MM. Light stamping lithography: microcontact printing without inks. *J Am Chem Soc* 2006;**128**:858–65.
155. Lee BH, Sung MM. Selective atomic layer deposition of metal oxide thin films on patterned self-assembled monolayers formed by microcontact printing. *J Nanosci Nanotechnol* 2007;**7**:3758–64.
156. Heule M, Schönholzer UP, Gauckler LJ. Patterning colloidal suspensions by selective wetting of microcontact-printed surfaces. *J Eur Ceram Soc* 2004;**24**:2733–9.
157. Marzolin C, Terfort A, Tien J, Whitesides GM. Patterning of a polysiloxane precursor to silicate glasses by microcontact printing. *Thin Solid Films* 1998;**315**:9–12.
158. Jacobs HO, Whitesides GM. Submicrometer patterning of charge in thin-film electrets. *Science* 2001;**291**:1763–6.
159. Cao TB, Xu QB, Winkleman A, Whitesides GM. Fabrication of thin, metallic films along the sidewalls of a topographically patterned stamp and their application in charge printing. *Small* 2005;**1**:1191–5.
160. Liang S, Chen M, Xue QJ, Liu ZL. Micro-patterning of TiO_2 thin films by photovoltaic effect on silicon substrates. *Thin Solid Films* 2008;**516**:3058–61.
161. Collins RJ, Shin H, De Guire MR, Heuer AH, Sukenik CN. Low temperature deposition of patterned TiO_2 thin films using photopatterned self-assembled monolayers. *Appl Phys Lett* 1996;**69**:860–2.
162. Lipowsky P, Hoffmann RC, Welzel U, Bill J, Aldinger F. Site-selective deposition of nanostructured ZnO thin films from solutions

containing polyvinylpyrrolidone. *Adv Funct Mater* 2007;**17**:2151–9.
163. Masuda Y, Kato K. Liquid-phase patterning and microstructure of anatase TiO_2 films on SnO_2:F substrates using superhydrophilic surface. *Chem Mater* 2008;**20**:1057–63.
164. Masuda Y, Sugiyama T, Seo WS, Koumoto K. Deposition mechanism of anatase TiO_2 on self-assembled monolayers from an aqueous solution. *Chem Mater* 2003;**15**:2469–76.
165. Koumoto K, Seo S, Sugiyama T, Seo WS, Dressick WJ. Micropatterning of titanium dioxide on self-assembled monolayers using a liquid-phase deposition process. *Chem Mater* 1999;**11**:2305–9.
166. Shirahata N, Masuda Y, Yonezawa T, Koumoto K. Control over film thickness of SnO_2 ultrathin film selectively deposited on a patterned self-assembled monolayer. *Langmuir* 2002;**18**:10379–85.
167. Masuda Y, Saito N, Hoffmann R, De Guire MR, Koumoto K. Nano/micropatterning of anatase TiO_2 thin film from an aqueous solution by site-selective elimination method. *Sci Technol Adv Mater* 2003;**4**:461–7.
168. Masuda Y, Sugiyama T, Lin H, Seo WS, Koumoto K. Selective deposition and micropatterning of titanium dioxide thin film on self-assembled monolayers. *Thin Solid Films* 2001;**382**:153–7.
169. Gao YF, Masuda Y, Koumoto K. Micropatterning of TiO_2 thin film in an aqueous peroxotitanate solution. *Chem Mater* 2004;**16**:1062–7.
170. Masuda Y, Jinbo Y, Yonezawa T, Koumoto K. Templated site-selective deposition of titanium dioxide on self-assembled monolayers. *Chem Mater* 2002;**14**:1236–41.
171. Masuda Y, Seo WS, Koumoto K. Selective deposition and micropatterning of titanium dioxide on self-assembled monolayers from a gas phase. *Langmuir* 2001;**17**:4876–80.
172. Saito N, Haneda H, Seo WS, Koumoto K. Selective deposition of ZnF(OH) on self-assembled monolayers in Zn–NH_4F aqueous solutions for micropatterning of zinc oxide. *Langmuir* 2001;**17**:1461–9.
173. Shirahata N, Masuda Y, Yonezawa T, Koumoto K. Atomic scale flattening of organosilane self-assembled monolayer and patterned tin hydroxide thin films. *J Eur Ceram Soc* 2004;**24**:427–34.
174. Gao YF, Masuda Y, Koumoto K. Micropatterning of lanthanum-based oxide thin film on self-assembled monolayers. *J Colloid Interface Sci* 2004;**274**:392–7.
175. Masuda Y, Wakamatsu S, Koumoto K. Site-selective deposition and micropatterning of tantalum oxide thin films using a monolayer. *J Eur Ceram Soc* 2004;**24**:301–7.
176. Gao YF, Masuda Y, Yonezawa T, Koumoto K. Site-selective deposition and micropatterning of zirconia thin films on templates of self-assembled monolayers. *J Ceram Soc Jpn* 2002;**110**:379–85.
177. Masuda Y, Kinoshita N, Sato F, Koumoto K. Site-selective deposition and morphology control of UV- and visible-light-emitting ZnO crystals. *Cryst Growth Des* 2006;**6**:75–8.
178. Saito N, Haneda H, Sekiguchi T, Ohashi N, Sakaguchi I, Koumoto K. Low-temperature fabrication of light-emitting zinc oxide micropatterns using self-assembled monolayers. *Adv Mater* 2002;**14**:418–21.
179. Saito N, Haneda H, Sekiguchi T, Ishigaki T, Koumoto K. Effect of postdeposition annealing on luminescence from zinc oxide patterns prepared by the electroless deposition process. *J Electrochem Soc* 2004;**151**:H169–73.
180. Saito N, Haneda H, Koumoto K. Pattern-deposition of light-emitting ZnO particulate film through biomimetic process using self-assembled monolayer template. *Microelectron J* 2004;**35**:349–52.
181. Nakanishi T, Masuda Y, Koumoto K. Site-selective deposition of magnetite particulate thin films on patterned self-assembled monolayers. *Chem Mater* 2004;**16**:3484–8.
182. Xiang JH, Zhu PX, Masuda Y, Koumoto K. Fabrication of self-assembled monolayers (SAMs) and inorganic micropattern on flexible polymer substrate. *Langmuir* 2004;**20**:3278–83.
183. Xiang JH, Masuda Y, Koumoto K. Fabrication of super-site-selective TiO_2 micropattern on a flexible polymer substrate using a barrier-effect self-assembly process. *Adv Mater* 2004;**16**:1461–4.
184. Gao YF, Masuda Y, Koumoto K. Patterning of ZrO_2 precursor through a gas-generated self-assembly route. *J Nanosci Nanotechnol* 2006;**6**:1842–6.
185. Yang P, Yang M, Zou SL, Xie JY, Yang WT. Positive and negative TiO_2 micropatterns on organic polymer substrates. *J Am Chem Soc* 2007;**129**:1541–52.
186. Peng Y, Shengli Z, Wantai Y. Positive and negative ZnO micropatterning on functionalized polymer surfaces. *Small* 2008;**4**:1527–36.
187. Liu CS, Masuda Y, Li ZW, Zhang Q, Li T. Site-selective growth of highly oriented ZnO rod arrays on patterned functionalized Si substrates from aqueous solution. *Cryst Growth Des* 2009;**9**:2168–72.
188. Masuda Y, Seo WS, Koumoto K. Deposition mechanism of anatase TiO_2 from an aqueous solution and its site-selective deposition. *Solid State Ionics* 2004;**172**:283–8.
189. Masuda Y, Yamagishi M, Koumoto K. Site-selective deposition and micropatterning of visible-light-emitting europium-doped yttrium oxide thin film on self-assembled monolayers. *Chem Mater* 2007;**19**:1002–8.
190. Kikuta K, Takagi K, Hirano S-I. Photoreaction of titanium-based metal–organic compounds for ceramic fine patterning. *J Am Ceram Soc* 1999;**82**:1569–72.
191. Kikuta K, Suzumori K, Takagi K, Hirano S-I. Patterning of tin oxide film from photoreactive precursor solutions prepared via the addition of N-phenyldiethanolamine. *J Am Ceram Soc* 1999;**82**:2263–5.
192. Hu XL, Masuda Y, Ohji T, Kato K. Micropatterning of ZnO nanoarrays by forced hydrolysis of anhydrous zinc acetate. *Langmuir* 2008;**24**:7614–7.
193. Pham TA, Kim P, Kwak M, Suh KY, Kim DP. Inorganic polymer photoresist for direct ceramic patterning by photolithography. *Chem Commun* 2007:4021–3.
194. Yoon TH, Lee HJ, Yan J, Kim DP. Fabrication of SiC-based ceramic microstructures from preceramic polymers with sacrificial templates and lithographic techniques – a review. *J Ceram Soc Jpn* 2006;**114**:473–9.
195. Nagata H, Ko SW, Hong E, Randall CA, Trolier-McKinstry S. Microcontact printed $BaTiO_3$ and $LaNiO_3$ thin films for capacitors. *J Am Ceram Soc* 2006;**89**:2816–21.
196. Ding L, Zhou WW, Chu HB, Jin Z, Zhang Y, Li Y. Direct preparation and patterning of iron oxide nanoparticles via microcontact printing on silicon wafers for the growth of single-walled carbon nanotubes. *Chem Mater* 2006;**18**:4109–14.
197. Lee BH, Cho YH, Shin H, Kim J, Lee J, Lee H, et al. Selective vapor-phase deposition of conductive poly(3,4-ethylenedioxythiophene) thin films on patterned $FeCl_3$ formed by microcontact printing. *Bull Korean Chem Soc* 2006;**27**:1633–7.